The Thesis Committee for Joseph Leo Selinger

Certifies that this is the approved version of the following Thesis:

Pilot Plant Modeling of Advanced Flash Stripper with Piperazine

APPROVED BY

SUPERVISING COMMITTEE:

Gary Rochelle, Supervisor

Eric Chen

Pilot Plant Modeling of Advanced Flash Stripper with Piperazine

by

Joseph Leo Selinger

Thesis

Presented to the Faculty of the Graduate School of

The University of Texas at Austin

in Partial Fulfillment

of the Requirements

for the Degree of

Master of Science in Engineering

The University of Texas at Austin

December 2018

Dedication

To my family

Acknowledgements

First of all, I would like to thank my parents and my brother for their unconditional love and support through all my years of schooling. Their support has helped me to grow and thrive, and I would be lost without their help and good judgment.

I would like to thank my research advisor, Dr. Gary Rochelle for his wisdom and support through my graduate program. While the work has been difficult, the knowledge I've gained is priceless. While working for him both as a graduate student and a teaching assistant I have learned about the many intricacies of carbon capture, as well as how to both a better teacher and a better student.

Of course, I would also like to thank Maeve Cooney for her unending help with editing and all administrative matters. Her feedback has helped not just me but the entire group to function, from managing the budgets for the constant trips to NCCC to not so gently cajoling us to turn in our quarterly progress reports.

I would also like to thank all the friends I have made in Austin, both in and out of the Rochelle group. I wish the best to all the senior graduate students who have gone on to illustrious careers, including Peter, Yu-Jeng, Yue, Ye, Darshan, Matt, Paul, Di, and soon Kent. I wish good luck to Korede, Yuying, Tianyu, and Ching-Ting as they continue working toward their PhD's. A special thanks to all my friends in Texas Table Top, who have helped keep me sane over the last few years. I will miss you all.

Finally, I would like to acknowledge the financial support of the Texas Carbon Management Program and the Cockrell School of Engineering Thrust 2000 Fellowship, who have provided the funds to help me conduct my research to complete my degree.

Abstract

Pilot Plant Modeling of Advanced Flash Stripper using Piperazine

Joseph Leo Selinger, MSE

The University of Texas at Austin, 2018

Supervisor: Gary Rochelle

Implementation of carbon capture using amine scrubbing is limited by the large energy penalty of CO_2 capture and compression. Alternative stripper designs can reduce lost work in the stripper by implementing heat recovery unit operations and reducing opportunities for solvent degradation. The advanced flash stripper (AFS) has reduced the required equivalent work by 12-15% compared to the simple stripper by using multiple solvent bypasses to equalize heat capacity across cross exchangers and minimizing lost latent heat of water vapor in the condenser.

The Advanced Flash Stripper using 5 m piperazine was studied at the National Carbon Capture Center (NCCC) pilot plant, which presented the novel opportunity to test the solvent and design configuration with coal-fired power plant flue gas. Piperazine (PZ) solvent was stripped of CO_2 with an average stripper operating temperature of 150 °C. The energy cost averaged 2.2 GJ/MT CO_2 for the AFS and 3.8 GJ/MT CO_2 for the simple stripper (SS).

A temperature-control heuristic for controlling bypass flowrates was evaluated using five AFS test cases. Using bypass temperature differences of 7 ℃, the bypass rates were automatically controlled to within 5% of the optimal bypass configuration. While the method was successful in simulations, unexpected heat loss in the NCCC plant limited the accuracy of the temperature-control heuristic due to the heat loss reducing the benefits of heat recovery unit operations.

Overall energy balances of the AFS using the Independence model showed a positive heat gain of 65000 Btu/hr. The unexpected heat gain was attributed to an overestimated heat of absorption in the Independence model, as well as an underestimation of the total heat transferred from the process steam. A test AFS run was analyzed using three different assumption methods, with energy requirements varying from 2.1 – 3.0 GJ/MT CO_2.

Table of Contents

List of Tables

List of Figures

Chapter 1: Introduction

1.1 CO_2 EMISSIONS

Coal-fired power plants are a major source of electricity worldwide, with over 1200 billion kilowatt-hours of electricity generated from coal in 2017 (EIA, 2018). Over a third of all emissions in the United States are produced from electricity generation, with 40% of the electricity produced by burning coal. While there has been a global trend to replace coal-fired processes with natural gas processes due to lower cost and reduced environmental impact, both methods significantly impact global climate change. Unlike cars with millions of individual internal combustion engines burning gasoline, electricity is produced at fixed point sources where the flue gas has the greatest concentration of CO_2. While some countries have installed multiple renewable energy plants to provide all or the majority of the country's energy requirements, there is still a need to provide fossil fuels for a portion of the energy crisis, and carbon capture offers benefits in capturing the otherwise lost emissions.

Figure 1.1 shows the estimated change in CO_2 emissions for petroleum, natural gas, and coal over the thirty years. Coal emissions have reduced by over 30% since 2000 due to the shutdown of old plants and a global change from coal to natural gas to satisfy consumer demand (EIA, 2018). However, CO_2 emissions from coal are expected to equalize from 2030-2050, including the shutdown of older plants that cannot reach the efficiency standards required by the EPA. Due to the high costs of plant shutdown and the availability of coal in the United States, there are feasible economic benefits to

choosing a carbon capture system (CCS) to capture CO_2 and either store it or use the CO_2 in another process such as enhanced oil recovery.

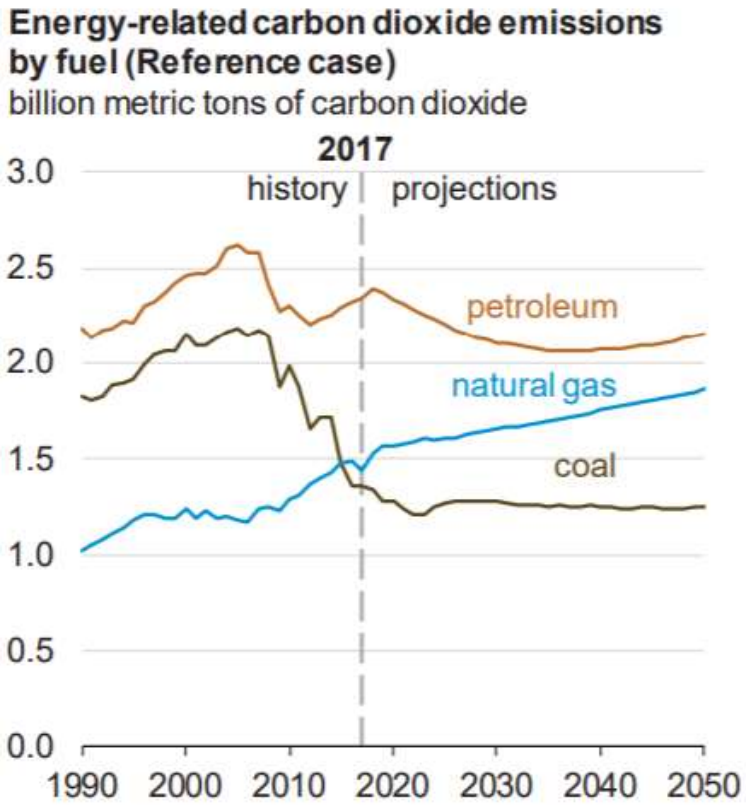

Figure 1.1: Predicted CO_2 emissions for different carbon suppliers

1.2 AMINE SCRUBBING

Carbon capture using amine scrubbing is a mature technology for removing CO_2 from flue gas, with the first design patent for the process dating back to 1930 (Bottoms, 1930). An example amine scrubbing process using the simple stripper configuration is shown in Figure 2. Flue gas containing between 3-20% of CO_2 is fed to an absorber

where 90% of the CO_2 is absorbed into a lean amine solvent at low pressure (1 bar) and low temperature (30 – 60 °C). The solvent, now rich with CO_2, is heated in a cross exchanger and fed to the stripper operating at high pressure (2 – 8 bar) and high temperature (120 – 170 °C) using steam to provide reboiler duty. The stripped lean solvent is then cooled in the cross exchanger and fed back to the absorber, forming a process loop. The CO_2 vapor exits the top of the stripper, is cooled to 40 °C to condense excess water vapor, and finally fed to a multi-stage compressor to be compressed to 150 bar.

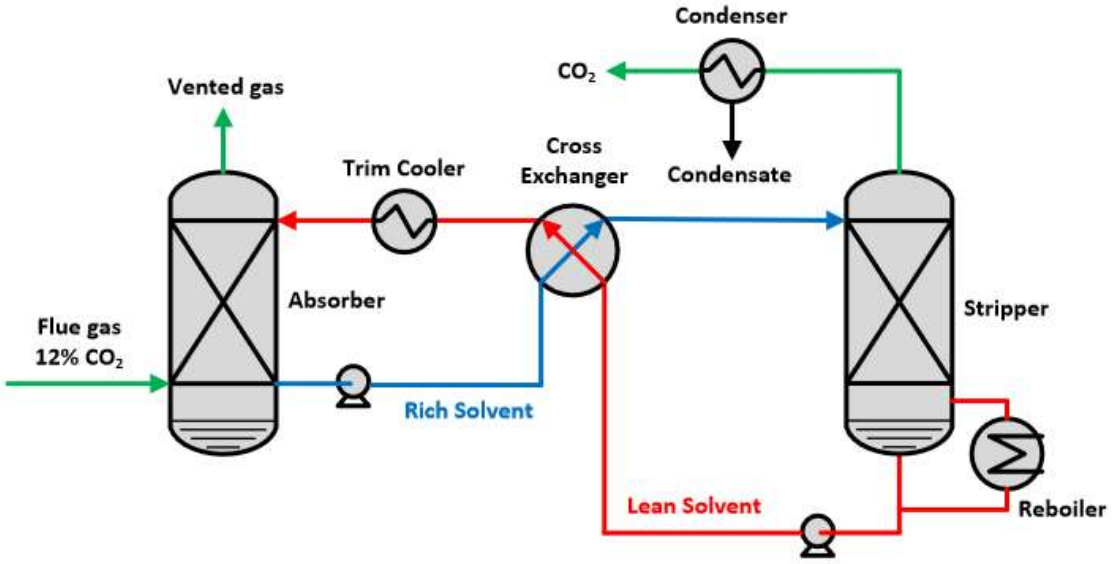

Figure 1.2: Amine scrubbing process with absorber and simple stripper

While carbon capture technology has been well-studied, the energy cost remains a significant barrier to wide-spread implementation. The energy penalty of carbon capture, including steam used in the stripper and electricity used in the compressor and pump,

requires 20-30% of the total electricity output of a power plant (Rochelle, 2009). Research on the amine scrubbing process has included a variety of methods to reduce costs and improve performance. Two of these methods are discussed in this paper: solvent degradation from NO_2 impurities and alternative stripper configurations to reduce energy costs.

1.3 SOLVENT DEGRADATION

While an ideal amine scrubbing process does not consume any amine from the solvent, degradation from multiple sources can increase operating costs as well as generate possible safety risks. A major source of amine loss is oxidative degradation, in which oxygen absorbed from the flue gas reacts with the solvent at stripper temperatures to degrade the amine (Voice, 2013; Nielsen, 2017). In addition, flue gas from coal plants frequently contains trace SO_x and NO_x impurities that can neutralize the parent amine, requiring both reclaiming to remove the degraded amine byproducts and additional make-up solvent to maintain the absorber/stripper loop. SO_2 impurities can form aerosols of water and amine that must be scrubbed to prevent undesired discharges of amine aerosol to the atmosphere (Beaudry, 2017). This project specifically focuses on the risks from NO_2, which can react with secondary amines to form nitrosamines, a carcinogenic degradation product (Garcia, Keefer, and Lijinsky, 1970). Preventing the accumulation of nitrosamines requires both thermal decomposition in the stripper and effective prescrubbing of the flue gas to remove NO_2 and prevent initial nitrosamine formation (Sapkota, 2015).

1.4. STRIPPER DESIGN CONFIGURATIONS

Alternative designs for the stripper have been proposed that reduce the net energy usage of the stripper. The estimated minimum equivalent work required for stripping and compression is approximately 19 kJ/mol CO_2, with the remaining work lost due to equipment working below 100% efficiency and imperfect heat recovery (Lin, 2016; Madan, 2013). Testing has included both the simulation of different configurations using Aspen Plus® and the Independence model, as well as the UT Austin Separation Research Program (SRP) pilot plant directly testing promising configurations (Plaza, 2011; Van Wagener, 2011; Sachde, 2016; Chen, 2017). The stripper configurations tested have included the simple stripper, the 2-stage flash with and without cold bypass, the 1-stage flash with cold bypass, and the advanced flash stripper. The 2-stage flash configuration is shown in Figure 1.3. The pilot plant solvents have included 9 m monoethanolamine (MEA) as well as 5 m and 8 m piperazine. Multiple piperazine solvent concentrations were tested to measure the effect of viscosity on heat and mass transfer performance. This work summarizes the results of the newest pilot plant test completed at the National Carbon Capture Center (NCCC) using the advanced flash stripper and authentic coal-fired power plant flue gas.

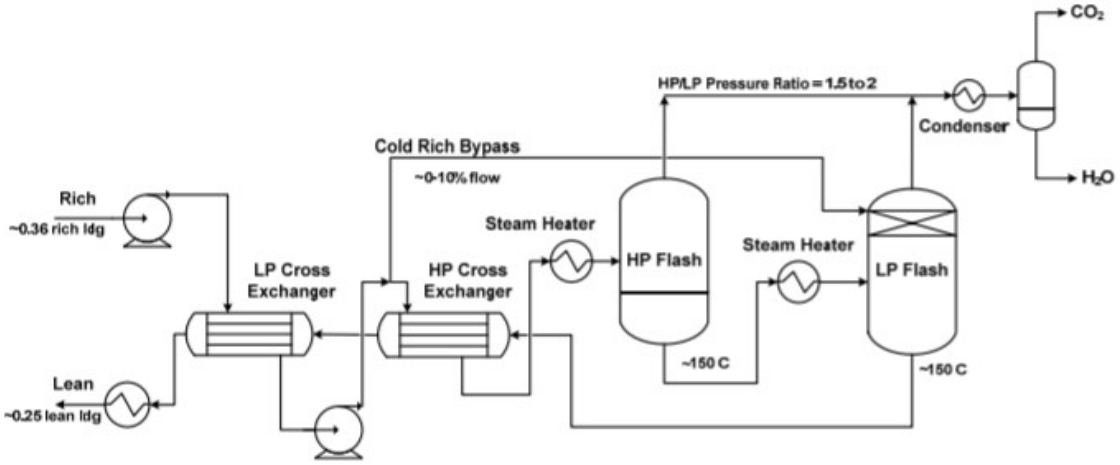

Figure 1.3: 2-stage flash stripper configuration with cold bypass

1.5 RESEARCH SCOPE

This work builds upon previous bench-scale testing of NO_2 removal and pilot plant testing of the advanced flash stripper by testing both designs at the NCCC pilot plant. Each additional test completed at a larger scale provides new information on the commercial feasibility of the process as a long-term mechanism to reduce global CO_2 emissions and reduce the effects of climate change.

The removal of NO_2 from flue gas using sulfite and thiosulfate is expanded from bench-scale measurements using synthetic flue gas (Sexton, 2018) to the use of an actual SO_2 polisher with a feed of 40 ppm SO_2. The effects of sulfite, thiosulfate, and pH are all measured to determine the requirements for steady-state removal of 90% of NO_2 in the flue gas.

A summary of the AFS model using Aspen Plus® is created, summarizing the choice of 5 m PZ as the desired solvent and how to model the different unit operations using the available blocks and design specifications. Bypass rates are selected using different criteria and tested using a temperature-control design heuristic. The effect of different cold bypass flowrates is further explored in the context of heat loss and the benefits of heat recovery specific to the AFS design.

Lastly, this work covers the NCCC testing of the advanced flash stripper using 5 m PZ for the first time, including initial test case analysis using the Aspen Plus® model. Heat exchanger performance is modeled based on solvent rate and pressure drop, and the energy requirement per ton of CO_2 captured is calculated. Multiple methods of modeling an individual test case are considered which each examine different limitations of the model and possible opportunities for data reconciliation.

Chapter 2: Stripper Modeling Methods

This chapter covers the methods used to model the Advanced Flash Stripper in Aspen Plus®. A summary will be provided of the individual unit operations used in the AFS, as well as the specifications used to match results to pilot plant data and implement new process correlations into the overall design. A summary of the pilot plant results using the AFS is provided in Chapter 4.

2.1 SOLVENT MODEL

Simulations were performed using Aspen Plus® version 8.8. The solvent chemistry - including CO_2, water, amine, and amine carbamate - was calculated using the electrolyte Non-Random Two-Liquid (e-NRTL) property method. The stripper column was simulated using the Independence Piperazine model using Aspen Plus RateSep® including regressions for thermodynamic and kinetic properties calculated based on experimental measurements of amine solvent properties (Frailie, 2014).

All amine scrubbing experiments in this work were conducted using 5 m piperazine (30 wt%). Piperazine is a 2nd generation solvent that has been well-studied as replacement for the standard industrial solvent monoethanolamine (MEA). Tests of 8 m PZ (40 wt%) showed a CO_2 absorption rate double that of 7 m MEA, as well as increased resistance to thermal and oxidative degradation (Chen, 2014, Freeman, 2011). By improving the resistance to thermal degradation, stripper temperatures can be increased up to 150 °C without observing significant thermal and oxidative degradation, compared to the MEA maximum of 120 °C. Operation at increased stripper temperature allows the stripper pressure to be additionally increased, reducing the work required by the CO_2

compressor. Recent studies have further shown 5 m PZ as a preferred solvent to 8 m PZ due to the reduced viscosity. By reducing the solvent viscosity, the mass transfer rate increases and the CO_2 absorption rate at 40 ℃ increases by an additional 30% (Chen, 2017; Song, 2018).

The Independence Piperazine model was developed by the Rochelle group and includes regressions for wetted area, vapor-liquid equilibrium, density, viscosity, solubility, diffusion coefficients and heat of absorption. The development of the Independence model is described in detail by Frailie (2014). While rate-based reactions are required when modelling the absorber, the stripper can be modelled with equilibrium reactions as the high temperature significantly increases the rate of all reactions. The amine-CO_2 reactions are listed below:

$$2PZ + CO_2 \rightleftharpoons PZH^+ + PZCOO^-$$

$$PZCOO^- + CO_2 + PZCOO^- \rightleftharpoons PZH^+ + PZ(COO)_2^{2-}$$

$$PZCOO^- + CO_2 + H_2O \rightleftharpoons H^+PZCOO^- + HCO_3^-$$

$$PZ + H^+PZCOO^- \rightleftharpoons PZH^+ + PZCOO^-$$

Diprotonated piperazine (PZH_2^{2+}) is not observed as a significant species in the solvent, though dicarbamate piperazine ($PZ(COO)_2^{2-}$) is.

2.2 Measurement Terminology

2.2.1 Loading

Amine loading is a measurement of the CO_2 absorbed by the solvent, defined as the moles of CO_2 per mole of alkalinity. The moles of CO_2 include all CO_2 captured in

carbamate form and bicarbonate formed. The exact speciation of the solvent will vary with increased loading, as free PZ reacts to form additional carbamate and protonated amine, as well as an increased concentration of dicarbamate. The moles of alkalinity vary between amines, as MEA as one mole equivalent alkalinity while PZ has two moles equivalent alkalinity per mole of amine. Piperazine is insoluble in water at low loading, so 5 m PZ requires a minimum lean loading of 0.18 to prevent crystallization at 40 ℃, a common absorber temperature due to the temperature of available cooling water. The difference between rich and lean loadings is referred to as the delta loading.

2.2.2 Equivalent Work

The energy requirement for the AFS is made up of three components: reboiler duty, compressor work, and pump work. The combined work term includes both the reboiler cost to strip the solvent, but also the energy requirement to compress the pure CO_2 to 150 bar for industrial storage and transport. The compressor work requirement is based on the inlet pressure of CO_2 gas received from the AFS, with an increased inlet pressure reducing the pressure ratio and the electricity requirement. The equivalent work equation is given below:

$$W_{eq}\left(\frac{kJ}{mol\ CO_2}\right) = 90\%\left(\frac{T_{stm} - T_{sink}}{T_{stm}}\right)Q_{reb} + W_{pump} + W_{comp}$$

The reboiler duty is converted into an estimated work requirement by multiplying by the isentropic efficiency of the steam turbine (Bhatt, 2011) and the Carnot cycle efficiency with T_{sink} = 373.15 K.

To reduce the simulation difficulty, the compressor is not directly modeled in the shown AFS models. A regressed empirical correlation used to estimate the compressor work is shown below (Madan, 2013; Lin, 2016).

$$W_{comp}\left(\frac{kJ}{mol\ CO_2}\right) = 15.3 - 4.6lnPin\ + 0.81(lnPin)^2\ - 0.24(lnPin)^3\ + 0.03(lnPin)^4$$

2.3 Advanced Flash Stripper – Overview

A general model of the AFS is shown in Figure 2.1. The development of the AFS design from the initial simple stripper configuration is described in detail by Lin (2016). This overview summarizes the key details of the AFS used to reduce the total energy requirement.

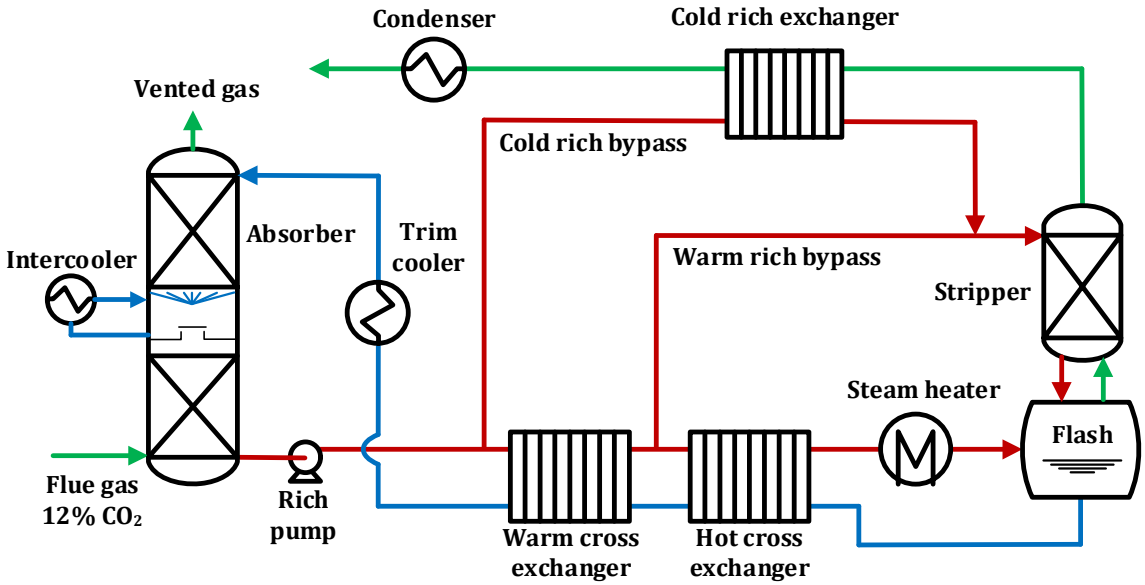

Figure 2.1: Advanced Flash Stripper design (Chen, 2017)

The simple stripper design uses a single rich stream heated in a single cross exchanger, then fed to the top of the stripper with a reboiler at the bottom heated with steam. The advanced flash stripper separates the cross exchanger into cold and warm exchangers, with a rich solvent bypass stream before each exchanger. The warm bypass stream contains between 25-45% of the rich solvent and is fed to the top of the stripper, with the balance fed to a steam heater at the bottom of the stripper that heats the solvent to the operating temperature. The cold bypass stream strips water from the vapor inside the stripper, reducing the water content in the hot vapor outlet to reduce energy loss in the condenser. The temperature of the warm bypass must be selected to minimize energy usage, as high temperatures increase the hot vapor water content, but low temperatures require additional steam duty to heat the solvent and may lead to reabsorption of CO_2 at the top of the stripper. Previous modeling has determined the solvent bubble point as the optimal bypass temperature (Lin, 2016). This design limits all rich solvent flashing to the warm cross exchanger, with the cold cross exchanger transferring only sensible heat.

The cold bypass makes up a smaller portion of the rich solvent, between 2-10% of the total rich flow. The cold bypass is used to recover heat in the cold rich exchanger from the hot vapor containing CO_2 and water (Van Wagener, 2011). The cold rich exchanger provides additional heat recovery for the AFS, including the heat of vaporization of water. The cold bypass receives no heat transfer from either cross exchanger, so the benefits of heat recovery from the hot vapor must be balanced with the heat recovery from the hot lean solvent. The heated cold bypass is combined with the warm bypass to form a single bypass stream that enters the top of the stripper.

The reboiler from the simple stripper is replaced with a steam heater followed by a flash tank to reduce solvent residence time and reduce oxidative degradation. The rich solvent separates into two streams: a hot vapor containing water and CO_2 and a lean solvent with the lean loading determined by the operating temperature and pressure. While the rich solvent has been effectively stripped in the flash tank, the hot vapor contains a large mole fraction of water. The sensible and latent heat of the water vapor, if not recovered, will be lost in the condenser which reduces the gas temperature to 40 ℃ and condenses water to produce a vapor that is 99% CO_2. The stripper provides direct contact heat recovery by contacting the vapor with warm bypass solvent, while the cold bypass exchanger provides indirect contact heat recovery with the cold rich bypass.

2.4 AFS MODEL

Figure 2.2 shows the advanced flash stripper modeled in Aspen Plus®. While the multi-stage compressor is not included in the model, the compressor work is estimated based on the correlation given in section 2.2.2 and used in the calculation of equivalent work.

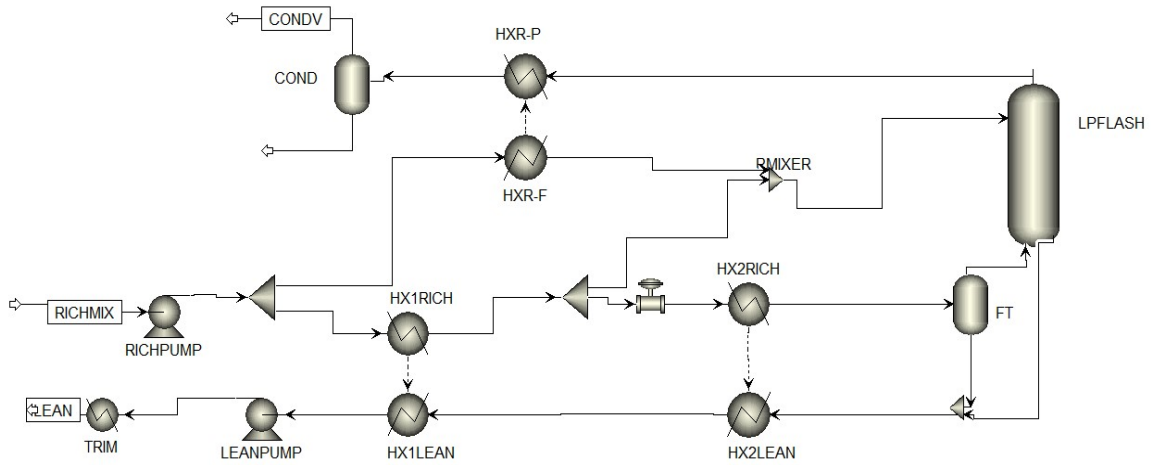

Figure 2.2: Advanced Flash Stripper Aspen Plus® model

The following sections describe how the individual unit operations of the AFS are modeled in Aspen Plus®, including design specifications.

2.4.1 Cross exchangers

2.4.1.1 Exchanger – simplified design

For the two cross exchangers and the cold bypass exchanger, each exchanger is modeled as a pair of heater blocks with a connecting heat stream. This is done to reduce the difficulty of model convergence compared to the more complex MHeatX block which provides a more complete analysis of the temperature change within the heat exchanger. Each heater block requires two specifications out of four options: outlet temperature, pressure drop, heat duty, or temperature change. The direction of the heat stream arrow is nontrivial when modeling the exchanger; the heat duty of the second heater block is equal

and opposite the duty of the first heater block, removing one degree of freedom. As an example, in Figure 2 the rich-end heater temperature and pressure drop are specified for the cold and warm heater blocks, with the heat duties specified for the lean-end heater blocks.

2.4.1.2 Heat transfer coefficient

While the double heater block method is simpler to converge, UA is not directly calculated unlike the MHeatX method. Setting the UA for the double heater block method in Aspen Plus® is done in two parts. First, a calculator block is used to calculate the log mean temperature difference (LMTD) for the two heater blocks, then determine the UA based on the specified or calculated heat duty. The same calculator block is also used to determine the correct UA based on correlations for the heat exchanger based on the solvent flow. Second, a design specification is used to match the actual UA to the correct UA by varying the outlet temperature or heat duty. If the heat duty or outlet temperature is overestimated, it is possible for the hot rich stream to exit at a higher temperature than the hot lean stream, which is not possible in reality. This causes the LMTD to be calculated as infinity, causing the simulation to throw an error. To prevent this, the initial guess of the exchanger heat duty must be underestimated to guarantee a feasible initial UA which can be improved with multiple iterations.

2.4.2 Steam heater and Flash Tank

The steam heater and flash tank are modeled as a single flash block with the stripper operating temperature specified. The flash block can be modeled with one of two configurations: the simplified model and the high temperature model shown in Figure 2.

In the simplified model, the stripper bottoms product feeds directly into the flash tank, which then provides a single lean solvent stream at the operating temperature. This method assumes perfect heat transfer between the hot rich feed and the hot lean bottoms, and the temperature of the vapor outlet to the bottom of the stripper is exactly the operating temperature. This method only includes a single operating temperature for the stripper sump, but does not reflect the realities of the actual steam heater configuration. Not only do the temperatures in the stripper sump not reach equilibrium, the rich solvent must be heated above the operating temperature since the lean solvent exiting the stripper is several degrees colder than the sump.

The high temperature model accounts for the variation in temperature within the sump by instead modeling the lean solvent using two streams: one exiting the flash tank and one exiting the stripper. The two streams are then mixed together to form the actual lean solvent flow, which is fed through the cross exchangers for heat recovery. The mixed stream is assumed to be at the operating temperature, an average of the hotter flash tank flow and the colder stripper flow. The temperature of the flash tank is determined using a design specification that varies the flash temperature to fit the mixed lean stream to the operating temperature.

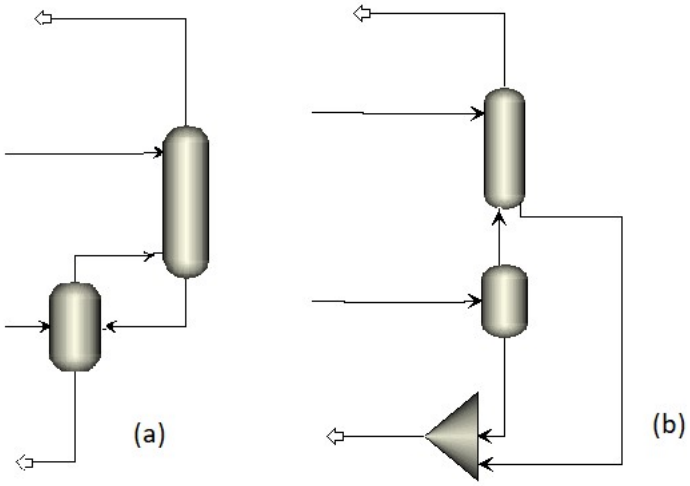

Figure 2.2: AFS stripper and flash tank, simplified model (a), high temperature model (b).

2.4.3 Stripper column

The stripper column is modeled with a RadFrac™ block with a liquid feed of warm bypass at the top and a vapor feed of water and CO_2 at the bottom. The Independence model calculates the actual wetted area as approximately 15%, so an actual stripper built based on the model results would need a height nearly seven times larger than predicted by the model. The amine is stripped of CO_2 primarily in the stripper sump, with the majority of the actual column used to strip water from the vapor to increase the CO_2 mole fraction. Increasing the height of the column effectively reduces the LMTD of the stripper, with greater heat transfer to the liquid feed. Existing Aspen Plus® models for the AFS do not include heat loss, so the temperature of the hot vapor exiting is bounded by the temperatures of both inputs. Chapter 4 will show how heat loss at the pilot scale can change these results due to heat loss in the top of the stripper and the pipe length.

2.4.4 Lean loading

Lean and rich loading, along with the solvent rate, are defined by the absorber performance. To achieve a specified lean loading, the temperature and pressure of the stripper must be modified. When designing the AFS the operating temperature is selected based on the thermal stability of the solvent, as well as the temperature of the available steam provided at the site. Given a fixed temperature, the lean loading is controlled by varying the stripper pressure. A design specification is used that maintains the lean loading by controlling the pressure in the flash tank, where the majority of CO_2 stripping occurs. To correct for the changing pressure, the pump pressure is recalculated based on the stripper pressure and any pressure drop through the main cross exchangers to provide the required discharge pressure.

2.5 ENERGY BALANCE

A full energy balance was developed for the pilot plant data shown in Chapter 4. The energy balance includes the inlet rich stream, outlet rich stream, CO_2 product and water condensate, steam, and cooling water. The rich solvent molality and rich loading were calculated based on the solvent density and viscosity, and was assumed to be accurate for the balance. The product flow was assumed to be pure CO_2 and measured with a flowmeter. A flowmeter for the liquid condensate existed, but did not provide accurate readings. To maintain the material balance, the lean solvent composition and flowrates were calculated based on the previous three streams. Aspen Plus® was used to calculate the enthalpy of each stream based on the given flowrates, temperatures,

pressures, and compositions. A summary of the energy balance results for the NCCC pilot plant campaign is given in Chapter 4.

Chapter 3: NO_2 Removal using Sulfite

3.1 Introduction

NO_2 impurities in flue gas may react with amines used in post combustion carbon capture to form nitrosamines. The formation of nitrosamines degrades the amine solvent, requiring makeup solvent and additional operating costs. While nitrosamine accumulation in the stripper can be limited using high operating temperatures and thermal reclaiming (Fine, 2015), neither method prevents the initial amine degradation from occurring, and both still require the disposal of oxidized byproducts. One low-cost solution takes advantage of the existing SO_2 polisher used to capture 99% of SO_2 in the flue gas. The formula for SO_2 absorption in the polisher is shown in Equation 1.

$$SO_2 + 2OH^- \rightarrow SO_3^{2-} + H_2O \quad (1)$$

NO_2 reacts with sulfite to form nitrite and sulfite free radicals (Equation 2), which in the presence of oxygen can cause a chain reaction forming multiple free radicals that eventually oxidize to sulfate or dithionate (Equations 3-6). This reaction occurs in the liquid boundary layer in the polisher and the reaction mechanisms were originally determined by Nash (1979) and Huie and Neta (1984).

$$NO_2 + SO_3^{2-} \rightarrow NO_2^- + SO_3^{\bullet -} \quad (2)$$

$$SO_3^{\bullet-} + O_2 \rightarrow SO_5^{\bullet-} \quad (3)$$

$$SO_5^{\bullet-} + SO_3^{2-} \rightarrow SO_4^{\bullet-} + SO_4^{2-} \quad (4)$$

$$SO_4^{\bullet-} + SO_3^{2-} \rightarrow SO_3^{\bullet-} + SO_4^{2-} \quad (5)$$

$$2SO_3^{\bullet-} \rightarrow S_2O_6^{2-} \quad (6)$$

Due to the formation of additional free radicals, multiple moles of sulfite are oxidized to capture a single mole of NO_2. To reduce the sulfite oxidation, an alternate reaction mechanism using thiosulfate as a free radical inhibitor was proposed by Owens (1984).

$$SO_5^{\bullet-} + S_2O_3^{2-} \rightarrow S_2O_3^{\bullet-} + SO_5^{2-} \quad (7)$$

$$SO_3^{2-} + SO_5^{2-} \rightarrow 2SO_4^{2-} \quad (8)$$

$$S_2O_3^{\bullet-} + S_2O_3^{\bullet-} \rightarrow S_4O_6^{2-} \quad (9)$$

To determine the feasibility of sulfite absorption with thiosulfate inhibitor for NO_2 absorption, experiments were carried out at the National Carbon Capture Center using coal-fired flue gas containing 40 ppm SO_2 and their existing SO_2 prescrubber with a 99% removal rate. This chapter covers the results of scrubbing 1-5 ppm NO_2 from flue gas, including the sulfite oxidation rate and the benefits of thiosulfate as a free radical scavenger.

3.2 EXPERIMENTAL METHODS

The pilot plant testing of the SO_2 polisher for NO_2 scrubbing was carried out using a 1300-gallon polishing scrubber with 9000 lb/hr of coal flue gas containing 12% CO_2, 7% O_2 and 40 ppm SO_2. Solvent was constantly circulated between the scrubber and a buffer tank at 1500 lb/hr, which was used for the addition of chemicals and solvent bleeding. Figure 3.1 shows a simplified drawing of the scrubber and buffer tank, including chemical addition and disposal. The pH was maintained between 7.5 and 10 using sodium hydroxide. The pH in the scrubber varied significantly due to intermittent addition of 10 wt% NaOH when the pH decreased below 8. The SO_2 in the flue gas was converted first to sulfite and subsequently oxidized to sulfate, with 99% SO_2 removal.

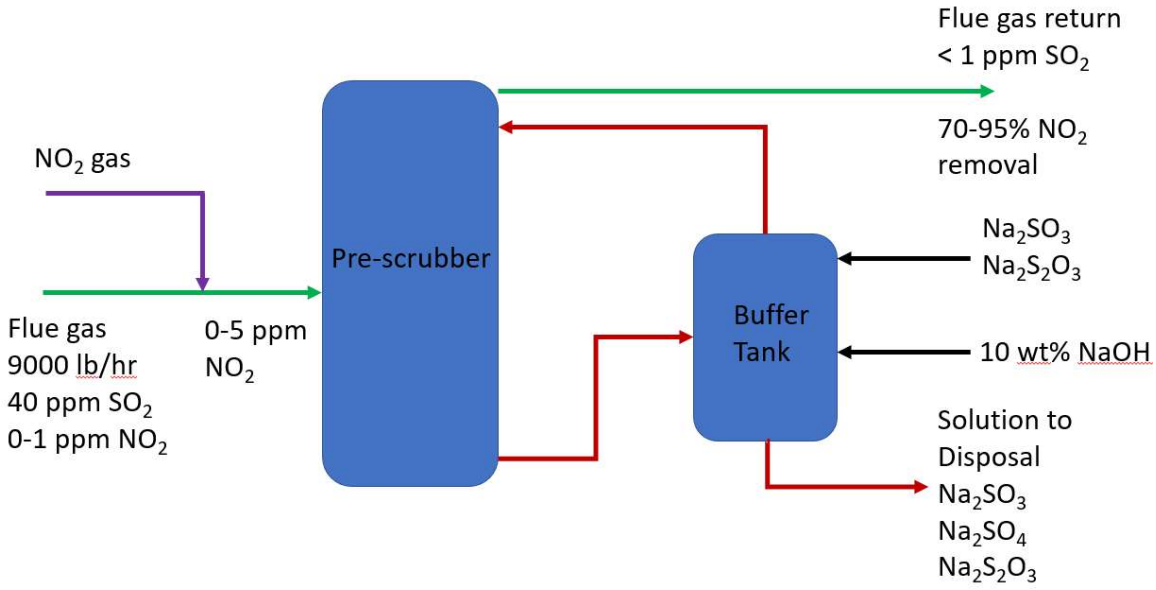

Figure 3.1: Process Flow Diagram of SO_2 polishing scrubber

The buffer tank level increased during the pilot plant campaign due to water condensation from the flue gas, which diluted the added sulfite and thiosulfate. The tank level was initially reduced to 30% when adding sulfite, thiosulfate, and EDTA, and maintained below 80%. The campaign was conducted in two parts. For the first week, flue gas was used containing 0-1 ppm NO_2 with no additives. For the following five weeks, supplemental NO_2 was added to the flue gas to increase the concentration to 3-5 ppm NO_2. The variation in flue gas concentration was due to the valve used to maintain the supplemental NO_2 flowrate, which was based on average flue gas flowrate and not controlled based on specific concentration.

Solid sodium sulfate, sodium thiosulfate pentahydrate, and EDTA were all purchased from Fischer Scientific and dissolved in water before adding to the buffer tank. After measuring the concentrations of the unmodified prescrubber solvent, the sulfite was increased to 22 mmol/kg, thiosulfate to 120 mmol/kg, and EDTA to 0.02 mmol/kg. Before adding the supplemental NO_2 after the first week of operation, additional thiosulfate was added to a concentration of 230 mmol/kg.

During the campaign, liquid samples were collected approximately once per day, with additional samples taken while adding chemicals. Samples were immediately mixed with 35 wt % formaldehyde at a ratio of 2 g formaldehyde / 10 g sample to completely react all sulfite to form methylsulfonic acid. The samples were shipped to Austin for additional analysis. To determine the rate of sulfite and thiosulfate oxidation, the liquid samples were analyzed using anion chromatography. The anion chromatography method and the bench-scale testing apparatus are both described in Appendix A.

3.3 RESULTS

3.3.1 Sulfite

The initial addition of thiosulfate significantly reduced oxidation within the prescrubber tank, leading to a net increase in sulfite over the first week of operation. During the first three days of operation, sulfite increased from 22 mmol/kg to 53 mmol/kg. Thiosulfate decreased over the first week due to both reacting with sulfite radicals and tank dilution due to water condensation in the flue gas. As thiosulfate decreased below 90 mmol/kg, the sulfite concentration reached a maximum at 52 mmol/kg, then decreased to 45 mmol/kg over the remainder of week 1.

During weeks 2-6, sulfite loss was first order with respect to sulfite as shown in Figure 3.2. The rate constant was 3.0 hr^{-1}, more than an order of magnitude greater than previous bench-scale experiments with rate constants of 50-400 hr^{-1} (Sexton 2018). The reduced rate constant was due to the feed of 40 ppm SO_2 in the flue gas, producing a constant sulfite feed that was unaffected by the concentration of either sulfite or thiosulfate.

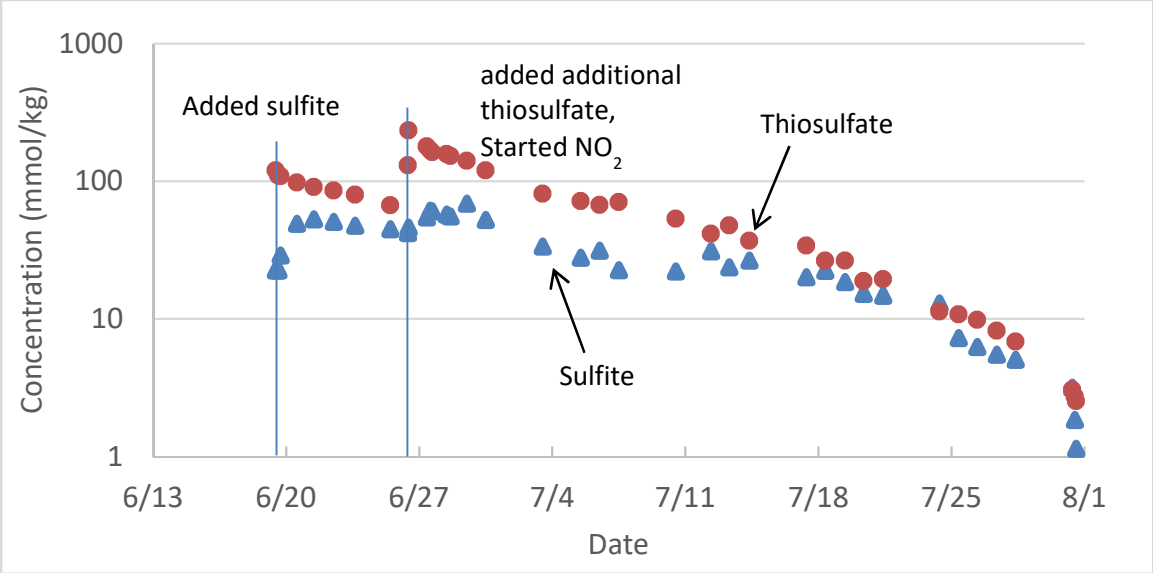

Figure 3.2: Sulfite and thiosulfate oxidation. 9000 lb/hr flue gas, 40 ppm SO_2.

3.3.2 NO_2 removal

The NO_2 inlet concentration was increased to 5 ppm at the beginning of week 3. Figure 3.3 shows the NO_2 removal and sulfite for weeks 2-6. The initial NO_2 removal was 95-98% using 35 mmol/kg. As the sulfite decreased to a minimum of 3 mmol/kg, the NO_2 removal decreased to 72%. While sulfite production in the prescrubber is approximately constant from the 99% SO_2 removal from the flue gas, the sulfite oxidation varies based on NO_2 and thiosulfate. As the thiosulfate becomes further diluted, sulfite oxidation becomes greater than sulfite production, and net sulfite decreases. Significant NO_2 removal was achieved at all levels of sulfite tested, removing over 70% of NO_2 using only 3 mmol/kg. Further research is needed at lower sulfite and higher NO_2 to measure the requirements to remove 50-70% of NO_2. Additional research is also

needed at reduced oxygen concentrations, which will further reduce the oxidation rate while not affecting sulfite production from SO_2.

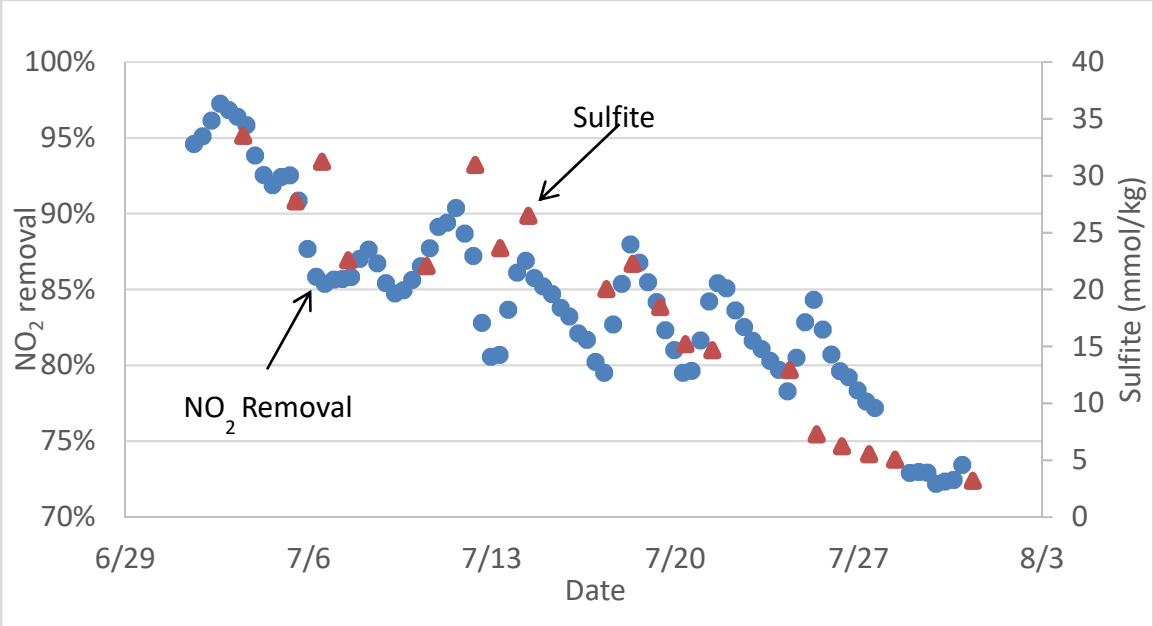

Figure 3.3: NO_2 removal decreases as sulfite oxidizes.

3.3.3 pH

As seen in Figure 3.3, NO_2 removal showed a clear cyclical trend, with an average period of 4 days. Figure 3.4 once again shows the NO_2 removal, now compared to pH. An increase in pH is immediately followed by an increase in removal that decays as the pH drops below 8. Increasing the pH by 1.5 points improves NO_2 removal by 5-8%, which was not correlated with sulfite or thiosulfate concentrations.

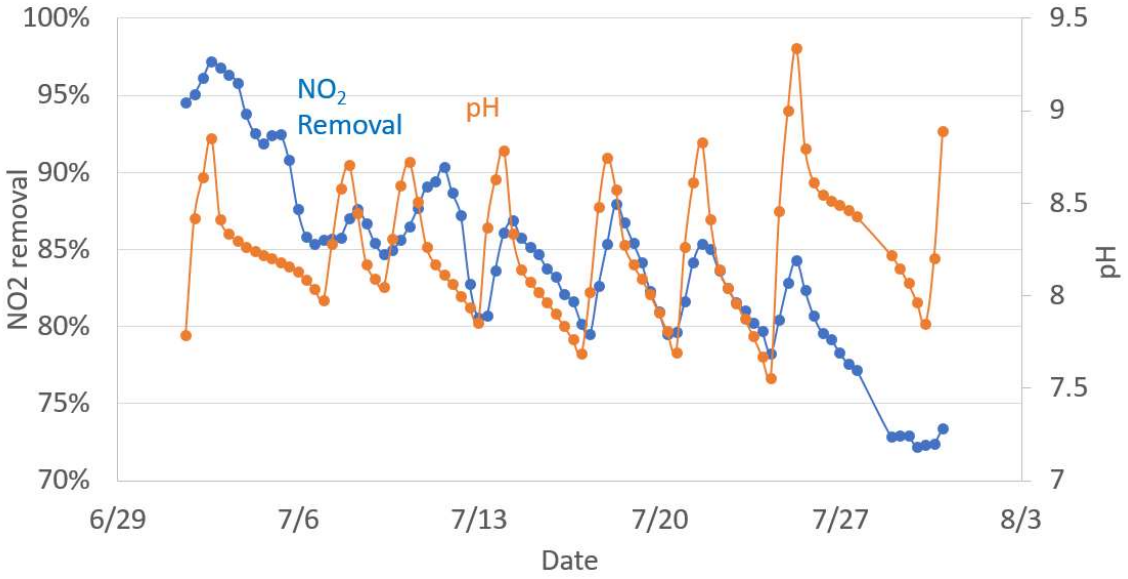

Figure 3.4: Cyclical NO_2 removal correlation with pH

The effect of pH on NO_2 removal has two probable explanations. First, the increased pH reduces the bisulfite/sulfite ratio. While both bisulfite and sulfite can react with NO_2, the bisulfite reaction is an order of magnitude slower than sulfite (Shen 1997). By replacing the bisulfite with sulfite, the overall NO_2 absorption rate of the prescrubber solvent increases. More testing is needed at a pH above 9 to determine the benefits of high pH operation. Second, the pH may directly affect the sulfite oxidation rate. A pH above 9 may reduce sulfite oxidation within the liquid film, increasing the sulfite in the film compared to the bulk solution.

3.3.4 Tank level

Due to condensed water in the flue gas, the liquid level in the prescrubber tank increased by 2-4% per day. Figure 3.5 shows the tank level in percent during the campaign, including multiple solution bleeds. The tank level was initially reduced to 30% at the beginning of week 1 while adding chemicals, then reduced to 30% again at the beginning of week 3. Instead of a constant solution bleed from the tank, the level was maintained by large intermittent bleeds to maintain a specific level. After adding chemicals at the beginning of week 2, the level was allowed to increase to 80%. The level was maintained between 60% and 80% for the remainder of the campaign. Additional spikes in level occurred when sodium hydroxide was added to maintain a pH over 8. The sulfate concentration was controlled by both solvent dilution and the intermittent bleeds.

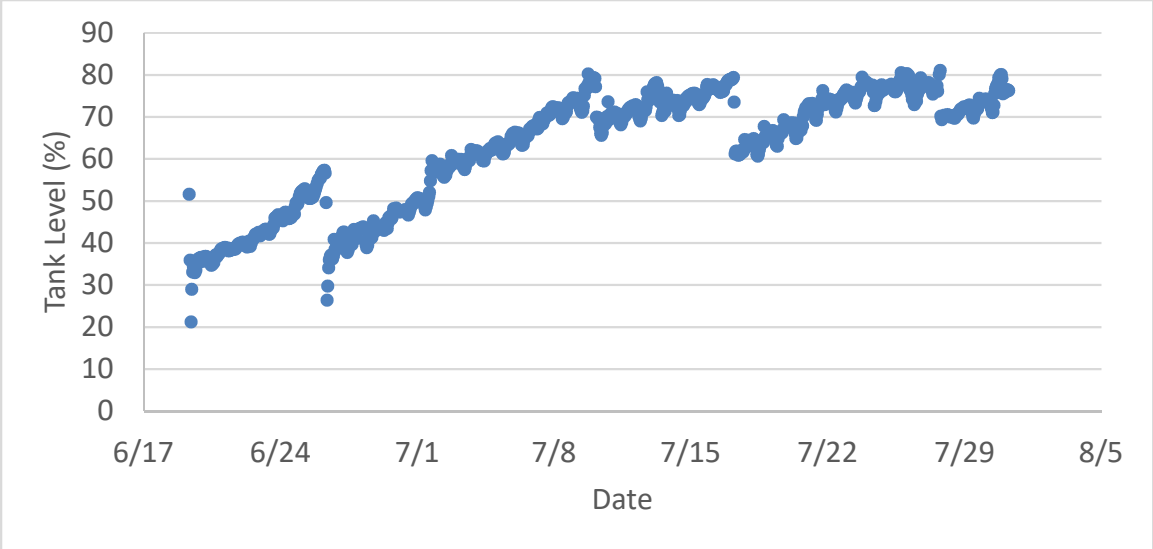

Figure 3.5: Prescrubber tank level and bleed

The loss of thiosulfate was due to both reactions with free radicals and tank bleeds. Figure 3.6 shows the total moles of thiosulfate from weeks 2-5. The prescrubber solution lost 260 moles of thiosulfate over 750 hours, with 60 moles of the loss attributed to solution disposal. An average of 0.27 mol/hr of thiosulfate was lost due to oxidation, accounting for over 75% of thiosulfate lost. For the given flue gas feed of 9000 lb/hr with 5 ppm NO_2, the replenishment rate for thiosulfate is 0.4 mol / mol NO_2. This corrsponds apporximately to the stoichiometry:

$2\ S_2O_3^{2-} + 2\ NO_2 \leftrightarrow 2\ S_2O_3^{-} + 2\ NO_2^{-}$

$2\ S_2O_3^{-} \leftrightarrow S_4O_6^{2-}$

$S_4O_6^{2-} + SO_3^{2-} \leftrightarrow S_3O_6^{2-} + S_2O_3^{2-}$

Overall:

$S_2O_3^{2-} + 2\ NO_2 + SO_3^{2-} \leftrightarrow 2\ NO_2^{-} + S_3O_6^{2-}$

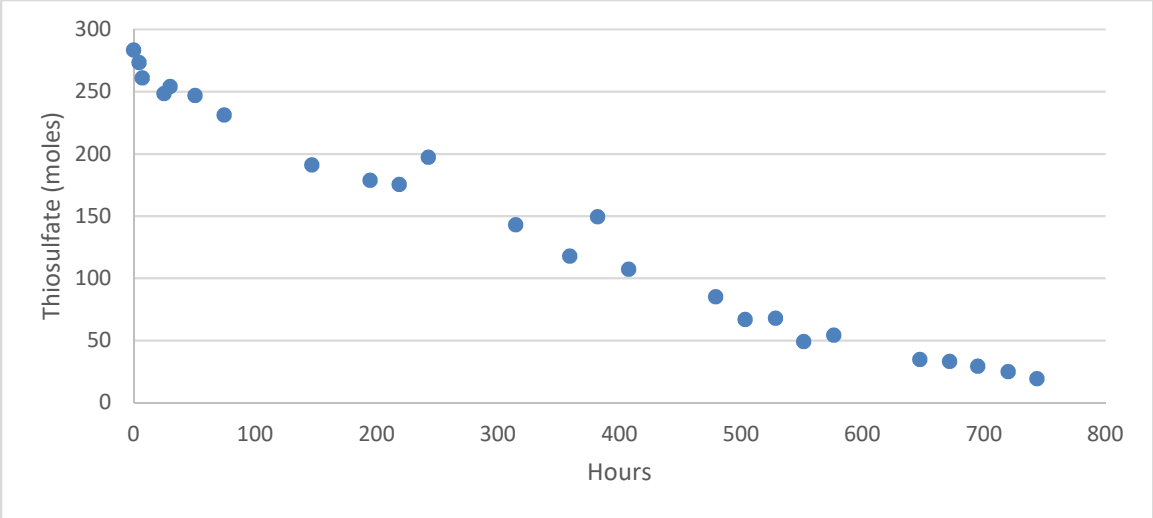

Figure 3.6: Total thiosulfate losses.

3.3.5 Removal requirements

In order to maintain a constant 90% removal of NO_2, the sulfite concentration must be maintained by reducing the oxidation rate below the rate of sulfite addition from flue gas SO_2. Varying thiosulfate adjusts the steady-state concentration of sulfite in the prescrubber, requiring makeup thiosulfate which was not tested in this campaign. Figure 3.7 shows a power law correlation between the thiosulfate concentration and the steady-state concentration of sulfite. The correlation was developed using a thiosulfate range from 5 to 180 mmol/kg. Doubling the thiosulfate increases sulfite by a factor of 1.6. The correlation is dependent on both SO_2 and NO_2 in the flue gas. Increasing SO_2 increases the rate of sulfite production and reduces the required thiosulfate, while NO_2 increases sulfite oxidation and requires additional thiosulfate. The effects of total gas flow are mixed, as additional NO_2 may lead to a rapid spike in sulfite oxidation. The correlation also assumes O_2 at 5-7%, which plays a key role in propagating the sulfite free radical reactions. The effects of reducing the O_2 below 5% are unclear: Shen predicted a proportional reduction in oxidation with O_2 concentration, while Fine predicted the oxidation rate would only decrease below 5% as the liquid boundary layer is depleted of oxygen. Bench-scale experiments conducted by Sexton et al. corroborate Shen, as reducing oxygen from 21% to 8% significantly reduced the oxidation rate.

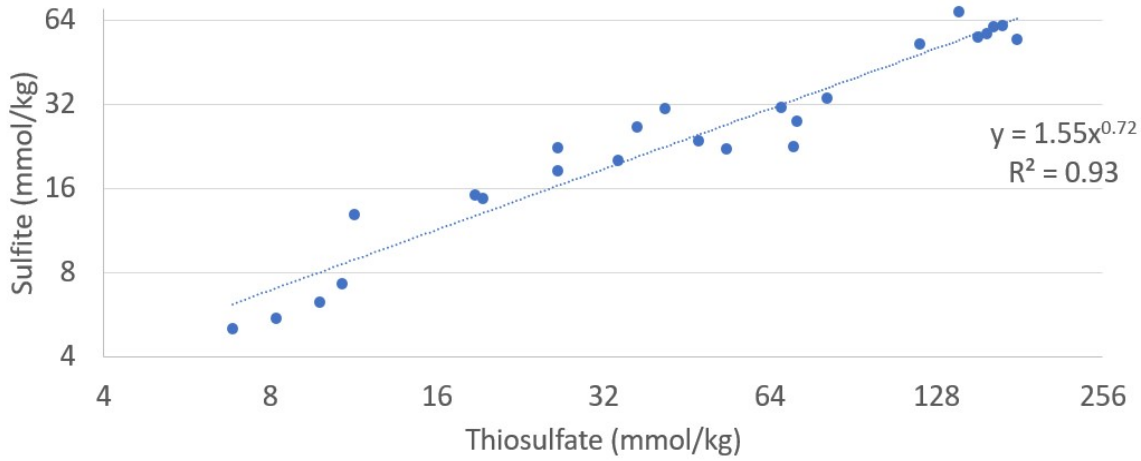

Figure 3.7: Steady-state sulfite correlation with thiosulfate, 40 ppm SO_2, 5 ppm NO_2.

The data in Figure 3.7 were collected at an average pH of 8.2, but actual pH varied from 7.5 to 9.5. As discussed previously, pH directly correlated with increased NO_2 removal regardless of sulfite and thiosulfate concentrations. Figure 3.8 shows the residuals of the sulfite-thiosulfate correlation correlated with pH. The correlation overestimates sulfite at low pH, and underestimates sulfite at high pH. The additional residual correlation suggests high pH significantly reduced sulfite oxidation. By increasing the pH in the prescrubber, a higher concentration of sulfite can be achieved without increasing thiosulfate.

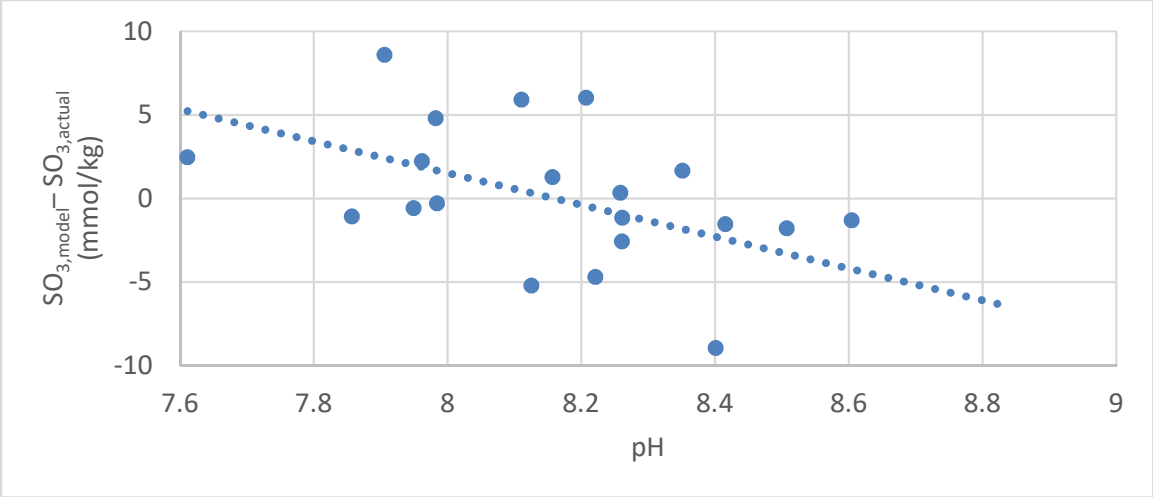

Figure 3.8: Residuals underestimate sulfite production at more basic conditions.

3.4 MODELING

3.4.1 NO_2 ABSORPTION

Fine (2015) analyzed NO_2 removal using sulfite oxidation with an average thiosulfate of 25 mM at 68 °C. Based on these results, Fine developed the following empirical model for NO_2 absorption:

$$NO_2\ absorbed\ \left(\frac{mol}{kg * min}\right) = \frac{(1 - e^{-N_{OG}})[NO_2]V}{m_{solution}}\left[\frac{1\ mol}{22.4\ L}\right]$$

Where N_{OG} = Number of gas phase transfer units; V = Feed gas molar flow; $m_{solution}$ = mass of sulfite solution.

The model assumes the reaction kinetics are controlled by mass transfer, with NO_2 rapidly reacting with sulfite in the liquid boundary layer. Solutions containing sulfite but no thiosulfate were not well fit by this model, as the sulfite in the boundary layer depleted rapidly, leading to reduced NO_2 absorption over the length of the experiment.

Additional bench-scale experiments were performed by Sexton et al. at increased temperatures, with an average temperature of 52 °C. This led to difficulties in measuring the NO_2 absorption rate, as increased temperature caused water to condense in the gas outlet stream which risked damage to the NO_2 analyzer. To account for the temperature effect, the empirical model was modified to include a temperature effect:

$$NO_2\ absorbed\ \left(\frac{mol}{kg * min}\right) = \frac{(1 - e^{-N_{OG}})[NO_2]V}{m_{solution}}\left[\frac{1\ mol}{22.4\ L}\right] * \exp\left(\frac{E_a}{R} * \left(\frac{1}{T_{ref}} - \frac{1}{T}\right)\right)$$

3.4.2 Sulfite oxidation rate

Sexton et al. further developed a model for the sulfite oxidation rate constant (k_{ox}) using both sets of bench-scale experiments. The model form is shown below with the regression parameters in Table 3.1 (Sexton, 2018):

$$k_{ox} = C_1\left(\frac{y_{NO2,feed}(1 - e^{-N_{OG}})}{y_{NO\ ,ref}}\right)^{X1}\left(\frac{[SO_3{}^{2-}]}{[SO_3{}^{2-}]_{ref}}\right)^{X2}\left(\frac{[S_2O_3{}^{2-}]}{[S_2O_3{}^{2-}]_{ref}}\right)^{X3}\left(\frac{[O_2]}{[O_2]_{ref}}\right)^{X4}\exp\left(\frac{E_a}{R} * \left(\frac{1}{T_{ref}} - \frac{1}{T}\right)\right)$$

Table 3.1: Regression parameters from oxidation model (Sexton, 2018)

Parameter	Regressed Model
C1	7.30
Ea (kJ/mol)	23.8
X1 (Nitrite)	0.55
X2 (Sulfite)	-0.05
X3 (Thiosulfate)	-0.39
X4 (Oxygen)	0.18

The expanded empirical model includes all relevant process variables expected to affect sulfite oxidation. Of particular interest is the limited effect of thiosulfate and oxygen found in the model. This is due to the majority of data using a minimum of 25 mM thiosulfate and 4% oxygen. While inhibited sulfite solutions reduce the number of moles of sulfite oxidized / mole of NO_2 absorbed by an order of magnitude compared to uninhibited solutions, there are rapidly diminishing returns with additional thiosulfate. A similar effect is seen for oxygen, with very low (<4%) O_2 in the feed gas significantly reducing sulfite oxidation which is not seen in the existing data set.

3.5 ALTERNATIVE INHIBITOR METHODS

The estimated cost of thiosulfate pentahydrate is $0.70/lb. Two alternative methods have been considered for further reducing this cost. The first method is direct

production of thiosulfate from colloidal sulfur. The reaction of sulfur with sulfite to produce thiosulfate is as follows:

$S + SO_3^{2-} \rightarrow S_2O_3^{2-}$

Initial testing using sulfur to produce thiosulfate have shown over 90% yield within 24 hours of addition, though sufficient agitation is needed to ensure the sulfur does not settle to the bottom of the vessel. Using sulfur may require a large initial feed of sulfite and thiosulfate to the prescrubber during start-up to ensure the reaction proceeds while NO_2 is absorbed. Without an initial feed of thiosulfate, the sulfite will oxidize to sulfate rather than react with the sulfur. To reach steady-state, the sulfite-thiosulfate correlation must be used to maintain the sulfite while the sulfur reacts with sulfite to produce more thiosulfate and further inhibit oxidation.

In design cases where the SO_2 feed is low, there may not be sufficient sulfite produced to effectively remove NO_2 regardless of inhibitor quantity. While NO_2 removal can still be conducted in the prescrubber, an alternate non-sulfite inhibitor is required. Fine showed tertiary amines provide effective oxidation inhibition by preferentially reacting with NO_2. Unlike sulfite, tertiary amines are not affected by oxygen-rich flue gas, providing additional benefits.

Chapter 4: NCCC Advanced Flash Stripper Testing

4.1 Introduction

Demonstrating the effectiveness of novel stripper configurations and solvents requires not only process modelling but also experimental results at the pilot scale. The pilot plant at the UT Austin Separations Research Program (SRP) has tested a variety of design configurations using piperazine, including the simple stripper, 1- and 2-stage flash with cold bypass, and the advanced flash stripper (Van Wagener, 2011; Lin, 2016; Chen, 2017). SRP completed two pilot plant campaigns using piperazine and the AFS; first in 2015 using 5m and 8m PZ and a flue gas containing 12% CO_2, then again in 2017 using 5m PZ and flue gas ranging from 4% to 20% CO_2. The SRP campaign results from 2015 have been discussed in depth by Lin, Chen, and Rochelle (2016), and the 2017 campaign results have been analyzed by Chen et al. (2017). The results from the NCCC pilot plant in this chapter have been previously published (Selinger, 2018).

4.2 AFS testing – SRP

The initial SRP test of the AFS was the first test of the new configuration, and showed reduced heat duty compared to previous designs and the benefits of a less viscous solvent on heat transfer. Figure 4.1 shows the reboiler heat duty of the 2015 SRP testing compared to previous tests over the past five years. The AFS showed a reduction of heat duty by 25% compared to the simple stripper, with heat duty ranging from 2.1-2.9 GJ/MT CO_2. Varying the cold and warm bypasses also determined that optimization of the bypass percentages could reduce heat duty by 5-15% (Lin, 2014).

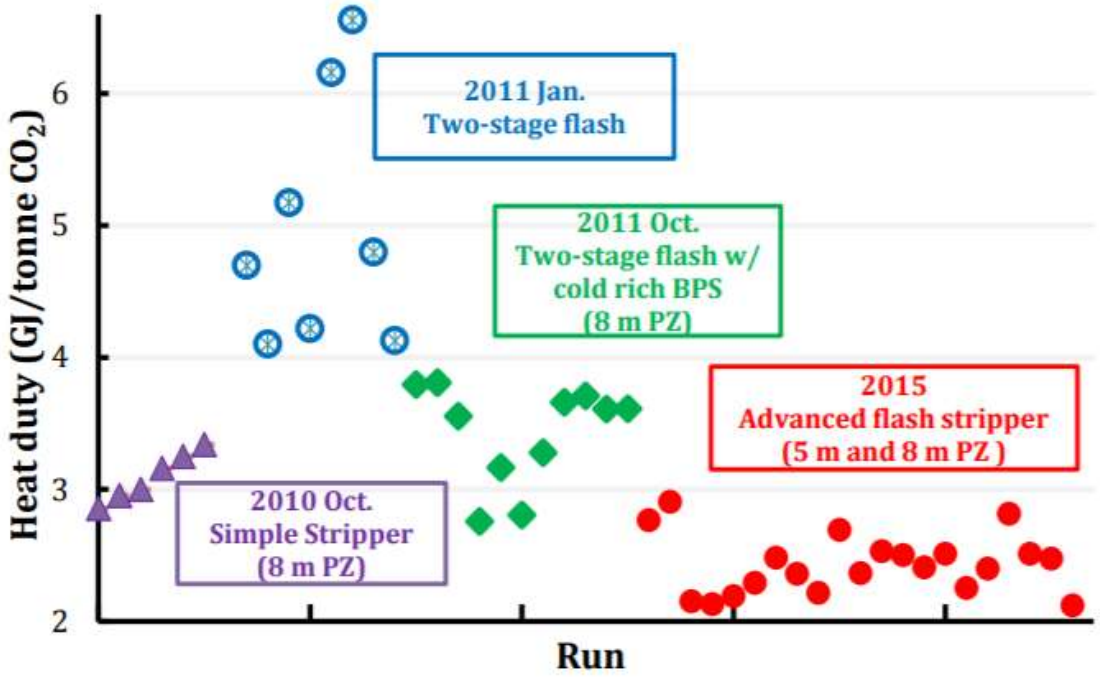

Figure 4.1: Comparison of heat duty between SRP tests

The SRP campaign in 2017 continued testing with the AFS configurations, now only using 5m PZ. Testing included three concentrations of CO_2 in the flue gas representing three design cases: 3.5% to represent natural gas-fired turbines, 12% for coal-fired power plants, and 20% for a new hybrid process combining membranes with amine scrubbing to produce a flue gas with increased CO_2 percentage. Since the stripper operating conditions are defined by the rich loading, lean loading, and solvent flowrate, the inlet CO_2 does not directly affect performance. However, reduced inlet CO_2 requires a lower lean loading and increased solvent flowrate to achieve the desired removal rate, which increases the required heat duty of the stripper.

Figure 4.2 shows the performance of the SRP 2017 AFS compared to test cases modeled in Aspen Plus®. Lean loading was strongly correlated with heat duty, with an average delta loading of 0.15. Reducing the lean loading from 0.24 to 0.18 while maintaining a constant AFS operating temperature of 150 ℃ required reducing the stripper pressure from 5.4 barg to 4.1 barg. The reduced pressure in the stripper reduces the CO_2 to water ratio in the stripper due to the changes in the heat of vaporization of water compared to the heat of desorption of CO_2. As the water content in the hot vapor exiting the stripper increases, more energy is lost in the condenser removing condensate, leading to increased overall energy costs.

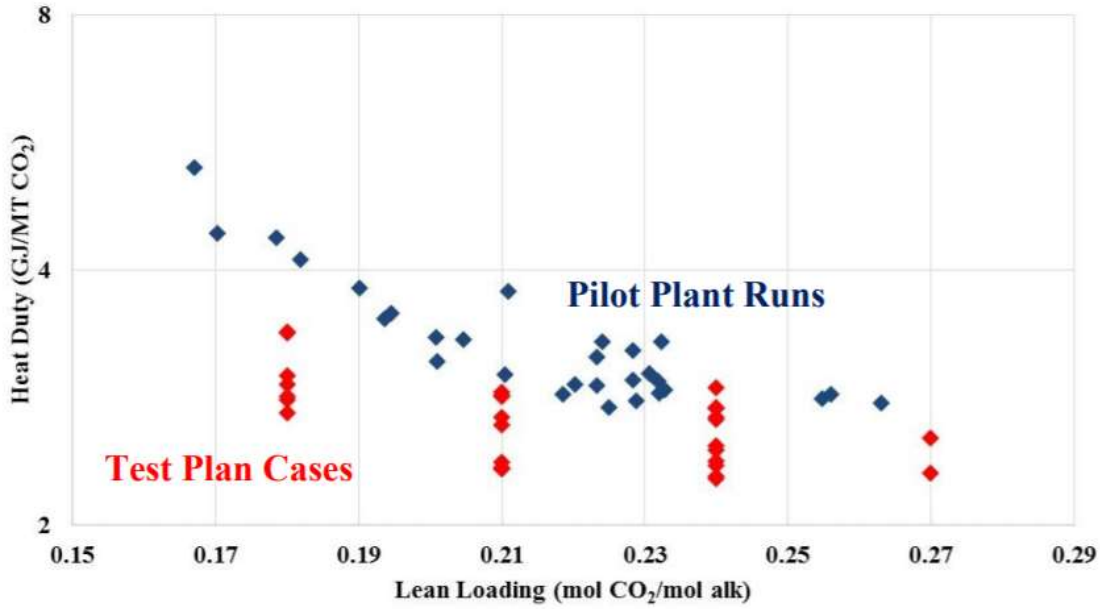

Figure 4.2: Heat duty of SRP 2017 compared to test cases

The test plan cases showed an average heat duty approximately 20% less than the actual pilot plant results. This difference includes the estimated heat loss of the stripper,

with increased solvent flowrates leading to increased heat loss. The heat loss as a percentage of total duty is expected to reduce as the process is further scaled-up to commercial size. In addition to heat loss, the model may have underestimated the energy requirements by underestimating the heat of desorption of 5 m PZ. A low heat of desorption solvent requires less energy to strip the CO_2 from the rich solvent, so the total energy requirement would be underestimated.

4.3 NCCC METHODS

4.3.1 NCCC vs SRP

The remainder of this chapter covers the testing completed at the National Carbon Capture Center (NCCC) pilot plant conducted between February to August 2018. The NCCC pilot plant is connected to the Gaston coal-fired power plant in Wilsonville, Alabama, which provided a fraction of the flue gas produced by an 880 MW coal boiler to the pilot plant. The NCCC pilot plant provided two key benefits compared to the SRP pilot plant testing previously completed. First, the flue gas directly represents the conditions of flue gas from a commercial coal plant, including trace NO_x, SO_x, and particulate. The SRP pilot plant uses a synthetic flue gas made up of air and CO_2, with SO_2 injected during some runs to test the formation of aerosols. Second, the NCCC plant provides an increased flowrate of flue gas, equivalent to 0.5 MW compared to SRP's 0.1 MW. Table 4.1 summarizes the differences between the NCCC design and the SRP design.

Table 4.1: Comparison of NCCC and SRP advanced flash stripper designs

	NCCC	**SRP**
Stripper diameter (in)	10	10
Stripper height (m)	4	2.25
Packing material	RSR 0.5, 0.7	RSR 0.5
Flue gas origin	Coal plant	Synthetic
Flue gas rate	0.5-0.6 MW	0.1 MW

4.3.2. Measurements

Data was collected from all instruments once per minute, and averaged over steady-state periods to define individual runs. CO_2 product flow was measured using a CO_2 flowmeter, though some data was lost due to intermittent plugging of the flow meter. The product flow was also estimated using the rich solvent flow, PZ molality, and delta loading. Molality and loading were calculated based on density, viscosity, and temperature using a regressed model for PZ loading (Freeman, 2011; Zhang et al., 2017). Due to a broken viscosity measurement on the lean stream, both molality and loading could not be directly determined for the lean return solvent. To calculate lean loading, the molality was assumed identical to the rich molality, and loading was calculated using only the density of piperazine. The density-viscosity correlation is listed below:

$$\rho_{PZ} = \rho_W * (0.0407 * C_{CO2} + .0008 * C_{PZ} + .991)$$

$$\mu = \mu_W * \exp[\left(\frac{26.16}{T} - .0265\right) * (7.69 * C_{PZ} - 7.80 * C_{CO} + 3.37 * C_{PZ} * C_{CO2})]$$

$$\mu_W = 2.41 * 10^{-5} * 10^{247.8/(T-140)}$$

ρ = density (kg/m^3); μ = viscosity PZ (cP); C = concentration (mol/kg); T = temperature (K)

Given density, viscosity, and temperature, the correlation system of equations can be solved.

4.4 NCCC TEST CASE MODELING

4.4.1 Test case plan

Before starting the NCCC campaign, test cases were simulated in Aspen Plus® to estimate the equivalent work and optimize the bypasses based on the Independence model. Table 4.2 lists five test cases analyzed, representing a range of conditions to be tested during the campaign. Case 1 represents the base case, with a lean loading of 0.24 and an operating temperature at 150 °C. Cases 2 and 3 reduce absorber temperature by 7 °C, which increases the CO_2 mass transfer driving force and requires less solvent to capture 90% of CO_2 in the flue gas. Cases 4 and 5 test the effects of stripper operating temperature between 128 °C to 165 °C, directly increasing pressure along with temperature to maintain lean loading.

Table 4.2: Test cases modeled in Aspen Plus®

Case	Description	RLDG	LLDG	Solvent flow (lb/hr)	Absorber product T (°C)	Stripper T (°C)
1	**Base Case**	0.39	0.24	15900	47	150
2	**Low absorber temperature**	0.41	0.24	13875	36	150
3	**Low absorber temperature, high LLDG**	0.41	0.27	16750	34	150
4	**High Reboiler Temperature**	0.41	0.24	13875	36	128
5	**Low Reboiler Temperature**	0.41	0.24	13875	36	165

4.4.2 Bypass Control

As discussed previously in Chapter 2, the advanced flash stripper adds two additional degrees of freedom in design: the cold and warm bypass percentages. While a minimum amount of bypass is required to provide sufficient liquid flow to the stripper column, optimizing the bypass ratios to minimize equivalent work requires significant

testing to determine and varies with changes to any process variable. While model optimization can be completed through multiple simulations, real-world testing is limited and an alternate heuristic must be developed to rapidly identify optimal or near-optimal bypass percentages.

Alternative process controls methods for the AFS were studied by Matt Walters (2016). Analyses of process control methods identify the temperature differences between hot vapor exiting the stripper and the bypass streams as process variables that can be controlled to minimize heat duty. Rather than set the mass flowrates for each bypass stream, the temperature differences would be specified and the mass flowrates controlled. One advantage of this method is the automatic readjustment of bypass flowrates as process changes are made, though this was not implemented in the design of the NCCC pilot plant. The temperature differences are referred to as DT1 and DT2 for the cold and total bypass streams. Figure 4.3 shows the temperature differences used for process control.

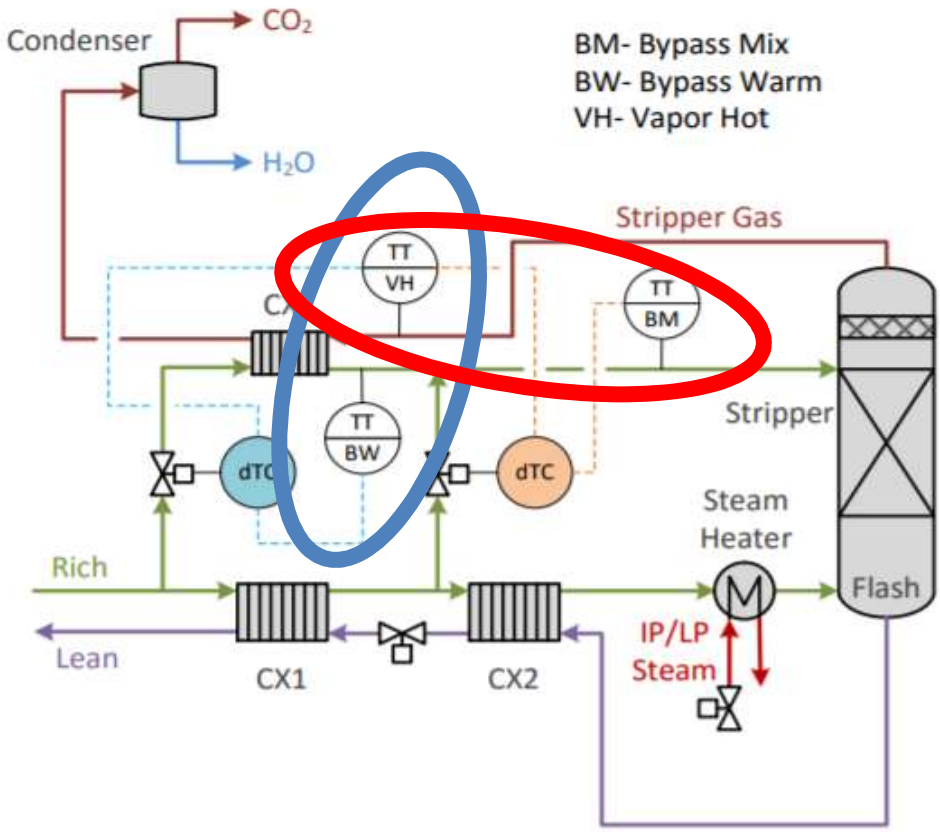

Figure 4.3: Temperature differences used to optimize bypass: DT1 (blue), DT2 (red) (Walters, 2016)

The temperature differences are calculated as follows:

$DT1 = T_{stripper\ gas} - T_{CX3\ Cold\ Outlet}$

$DT2 = T_{stripper\ gas} - T_{totalbypass}$

4.4.3 Test Case Results

The five test cases were modeled with two bypass calculation methods. First, each case was optimized to minimize equivalent work. Second, DT1 and DT2 were both assumed as 7 °C and the models were recalculated. Table 4.3 lists the bypass percentages for each case when using temperature control. When using DT1 and DT2 as controls, the mass flowrates varied significantly without the need to update the actual controls.

Table 4.3: Rich bypass controlled by temperature difference

Case Description	Cold bypass (%)	Warm bypass (%)
Base Case	7.8	26.9
Low absorber temperature	7.1	32.1
Low absorber temperature, high LLDG	4.6	18.7
High Reboiler Temperature	4.9	24.9
Low Reboiler Temperature	15.8	40.1

The bypass percentages vary significantly based on solvent loading and temperature. Both bypasses are minimized when operating at increased lean loading and increased temperature, and maximized when reducing temperature. Overall, the bypass

flow is dependent on the stripper pressure, with increased pressure raising the CO_2 to water ratio in the hot vapor. With less water trapped in the hot vapor exiting the stripper, less cold bypass is needed to recover the latent heat of steam.

Figure 4.4 compares the equivalent work from the temperature control cases to the actual optimized results. All temperature control cases showed similar performance to the optimized results, with the largest differences due to variations in operating temperature. While these tests suggest temperature control as a viable heuristic, the method is limited by several factors. First, the temperatures measured assumed no heat loss, which reduce temperature differences. Second, while 7 °C was assumed for both DT1 and DT2, it is not obvious these temperature differences are optimal for all process designs. Third, the NCCC plant required the bypass flow rates to be directly set by the operator and did not have control systems to vary the flow set points based on temperature differences.

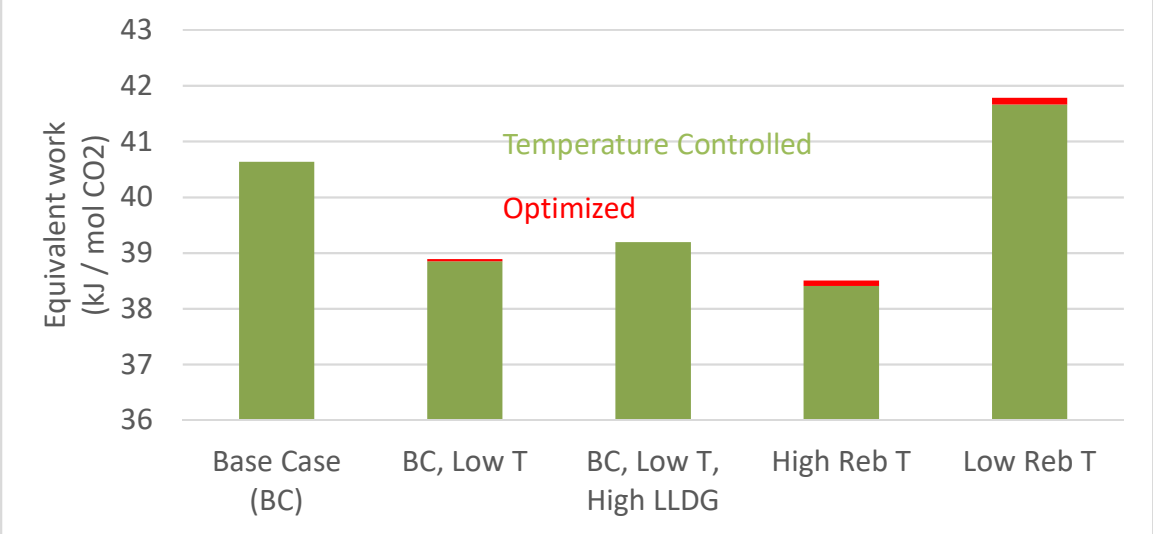

Figure 4.4: Equivalent work of test cases: optimized vs. temperature control

4.5 RESULTS

4.5.1 Experimental data collection

Data was collected from the NCCC pilot plant from January-August 2018, with several shutdowns due to repairs or reduced demand. After initial water testing, 600 hours of parametric testing with the AFS was completed. The simple stripper configuration was also tested for an additional 250 hours, using only the cold cross exchanger which limited available heat recovery. Finally, long-term testing with the AFS was conducted for 1350 hours before shutting down. Table 4.4 summarizes the AFS conditions tested during the campaign. Example AFS control system overview screenshots are included in Appendix B.

Table 4.4: AFS parameter test ranges

Parameter	Range
Lean Loading	0.20 – 0.27 mol/equiv PZ
Rich Loading	0.37 – 0.41 mol/equiv PZ
Solvent Flow	10000 – 20000 lb/hr
Stripper Temperature	133 - 155 °C
Stripper Pressure	35 – 92 psig
Cold bypass flow	500 – 1500 lb/hr
Warm bypass flow	2500 – 7200 lb/hr

4.5.2 Data limitations

When the temperature control heuristic was used in Section 4.4 to simulate NCCC performance, it was assumed that DT1 and DT2 would both be positive values. In a simulated design with no heat loss, this is by definition true: the hot vapor outlet temperature is between the temperature of the bypass and the stripper operating temperature. However, heat loss occurring in the AFS reduced DT2 far below expected, with an average DT2 of -4 compared to the expected value of 7 °C. This change limited the effectiveness of the temperature control heuristic.

Unlike the design of SRP, the temperature transmitter measuring the hot CO_2 vapor (TI40503) is not placed directly near the hot vapor outlet; rather, it is placed just before the cold bypass. Because of this difference in placement, two possible sources of heat loss are possible: heat loss in the column and heat loss in the pipe between the column and exchanger. If heat is lost in the column, additional water would be condensed and the CO_2 to water ratio of the vapor would increase. If heat is lost in the pipe, the additional water exits the top of the column but condenses in the pipe before the exchanger. Unfortunately, the flow rate of liquid condensate from the condenser was not accurately measured, so the water loss cannot be directly determined. Regardless of the heat loss source, the heat loss limits the benefits of heat recovery from the cold bypass exchanger. As seen in the test cases with high lean loading, reducing latent heat in the hot vapor reduces the required cold bypass flow.

4.5.3 Material Balance

The total CO_2 removal of the AFS can be calculated by two methods: the flow of product CO_2 exiting the AFS and the delta loading of the solvent multiplied by molality and solvent flow rate. Figure 4.5 shows the relative error of the measured CO_2 flow rate compared to the change in loading method over all AFS runs. The solvent and loading method used the density-viscosity correlation to determine both rich and lean loading. The solvent method of determining CO_2 flow effectively closed the material balance, with an average overestimate of 4%. The variation may be due to variations in the measurement of rich solvent flow, but the consistent positive overestimation suggests the density-viscosity correlation may require an additional multiplier to match the results to real data.

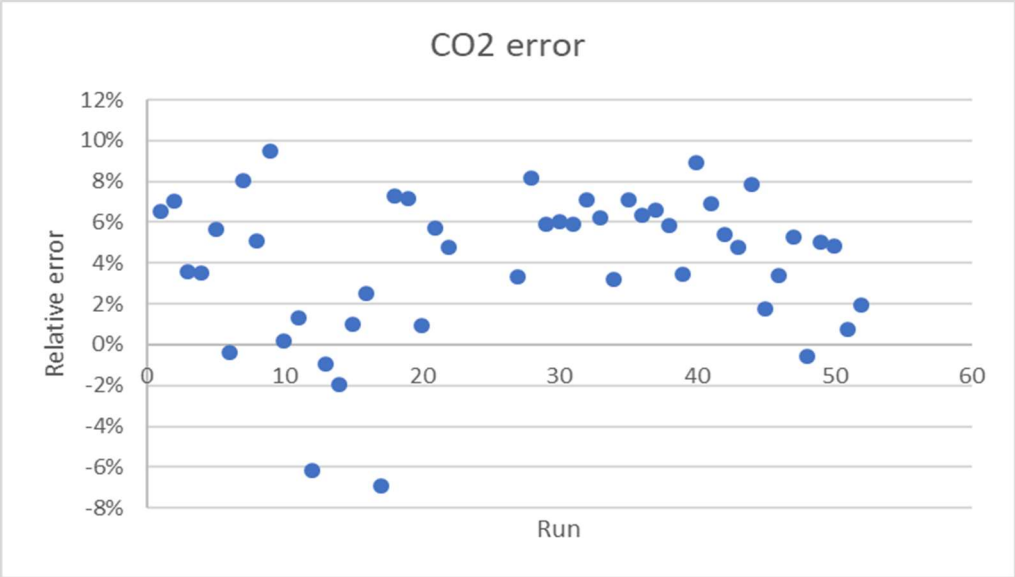

Figure 4.5: Overestimation of CO_2 mass balance by 4%. Relative mass balance error was calculated as $\%\ error\ = \frac{(m_{CO2,ldg} - m_{CO2,flowmeter})}{m_{CO2,flowmeter}}$. Solvent flow rate ranges from 10000 – 20000 lb/hr.

The majority of runs in the NCCC test plan included a lean loading of 0.24 mol/PZ equiv, with stripper temperature and pressure calculated to provide the desired lean loading. The required pressure was calculated using the Independence model in Aspen Plus®. Figure 4.6 compares the lean loading calculated by the Independence model to the lean loading calculated by the density-viscosity correlation. While the runs at low and high loading were similar for both methods, the correlation showed a greater variation of lean loadings between 0.21 and 0.25 mol/PZ equiv, while the Independence model limited the range of loadings between 0.23 and 0.24 mol/PZ equiv. It is additionally possible another variable beyond pressure and temperature must be considered when modelling runs, which would better match the model to match the actual

results. The lean loading may also be correlated with molality, which varied from 4.0 to 5.4 mol PZ / kg H_2O during the campaign. Reduced molality also reduces total CO_2 carried by the solvent, which may reflect in a lower estimated lean loading. The reduced molality also reduces the solvent viscosity, which may also have reduced the estimated lean loading by the density-viscosity correlation.

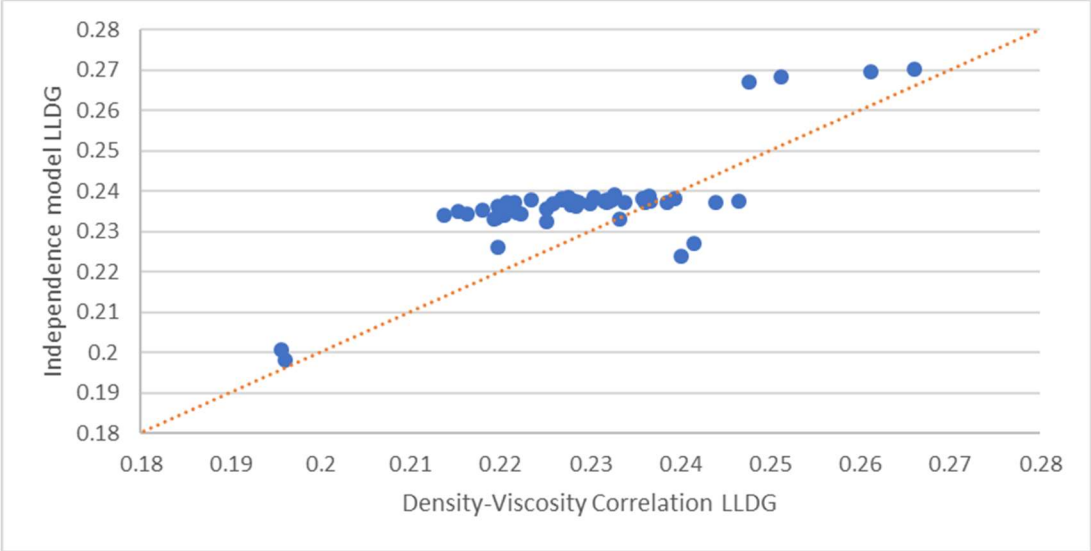

Figure 4.6: Lean loading range reduced when using Aspen Plus® for modeling

4.5.4 Heat Exchangers

4.5.4.1 Heat transfer coefficient

Accurate measurement of the heat transfer coefficient in the cross exchangers is a major element of AFS modeling, with a focus on correlating heat transfer coefficients with pressure drop and solvent flow. These correlations, when used in conjunction with

Aspen Plus®, allow for optimization of bypass rates and further testing of novel design cases. Figure 4.7 correlates heat transfer coefficients to solvent rate for the two cross exchangers, while Figure 4.8 does the same for the cold bypass exchanger. Both cold exchangers directly correlated heat transfer to solvent rate, with U increasing with average solvent rate by powers of 0.96 for the cold cross and 1.108 for the cold bypass. The direct correlation is expected as the solvent does not flash in either cold exchanger. All average flows for Figure 4.8 are clustered around 8 set points due to fixed solvent rate settings used for all runs. The hot exchanger, which includes some flashing in all runs, shows a reduced power-law correlation of 0.66, with heat transfer no longer directly scaling with solvent flow. Flashing within the exchanger leads to nucleate boiling, which is limited by the temperature approach.

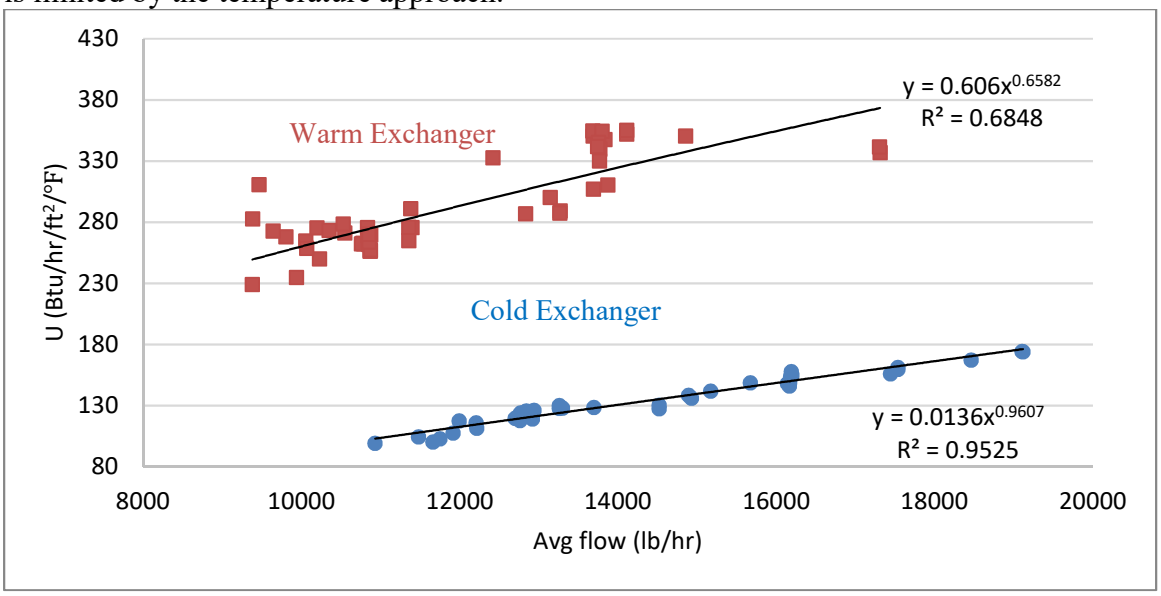

Figure 4.7: Cross exchanger heat transfer with direct correlation for cold exchanger. Cold cross exchanger area = 1227 ft^2. Warm cross exchanger area = 207 ft^2.

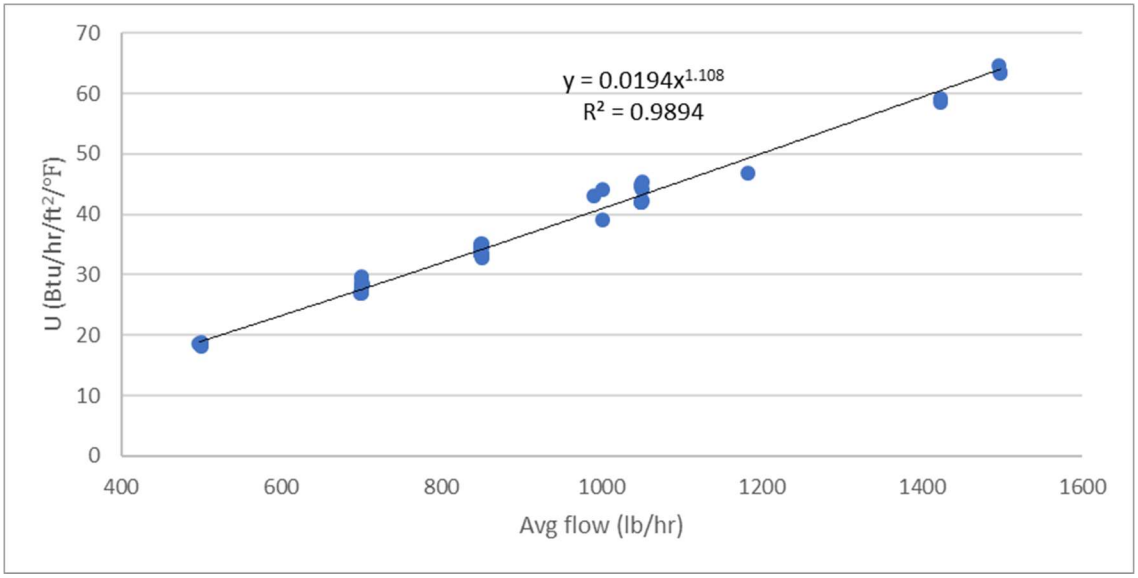

Figure 4.8: Bypass exchanger with lower U compared to cross exchangers due to liquid-gas exchange vs. liquid-liquid heat exchange in the cross exchangers. Bypass exchanger area = 91.5 ft^2.

4.5.4.2 Pressure drop

Selecting pressure drop in heat exchangers requires balancing heat transfer performance with increased capital and operating costs. As solvent flow increases, the fluid velocity causes additional turbulence within the exchanger, increasing both heat transfer and pressure drop. The optimum fluid velocity in the cross exchanger is dependent on the capital costs of the pump and heat exchanger as well as the cost of steam and electricity (Lin, 2016). Figures 4.9 and 4.10 show the increased heat transfer coefficient with respect to pressure drop for the cold and hot cross exchangers. As previously seen in Figure 7, the hot cross exchanger correlation is less accurate than the cold cross exchanger correlation due to flashing at high temperatures.

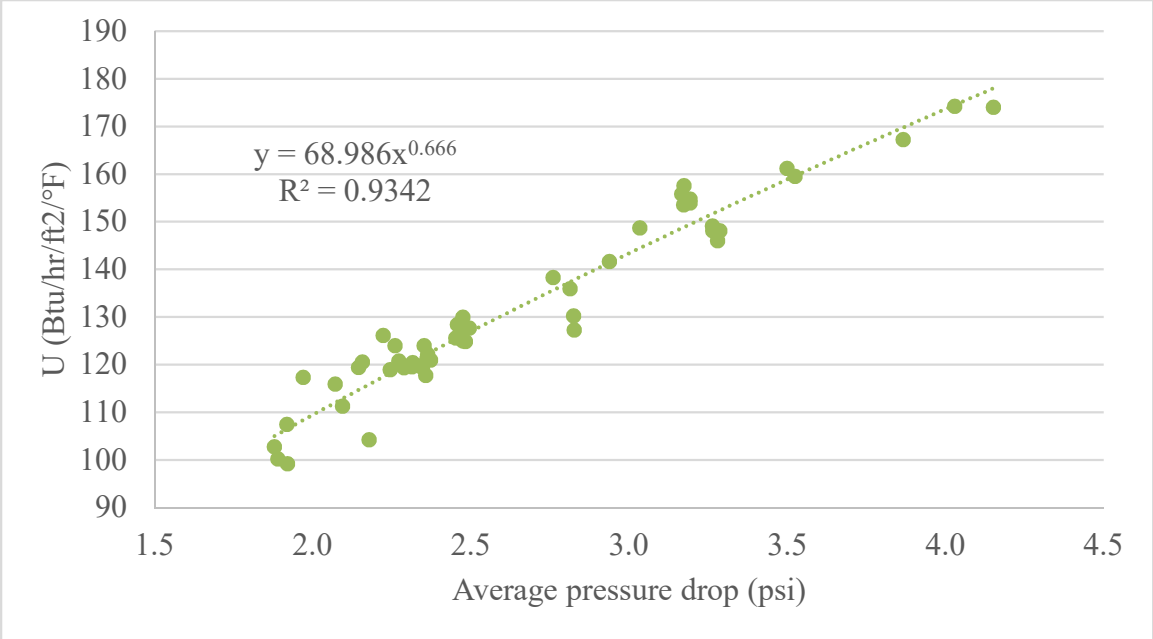

Figure 4.9: Heat transfer correlation with pressure drop for the cold cross exchanger

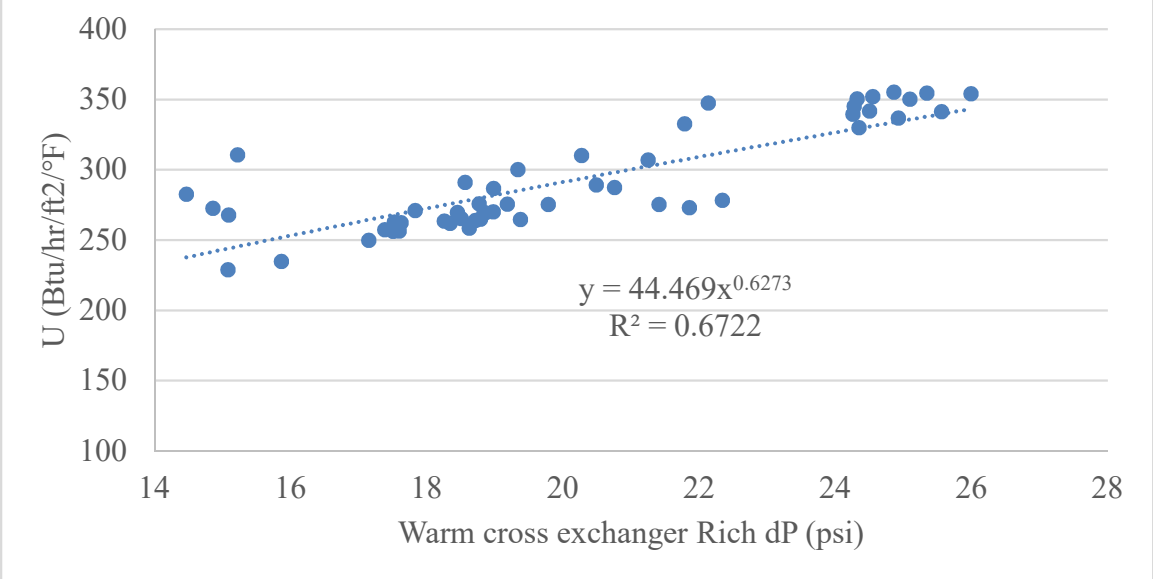

Figure 4.10: Heat transfer correlation with pressure drop for the hot cross exchanger

4.5.5 Heat duty

4.5.5.1 Experimental vs. model

The heat duty for the advanced flash stripper was calculated using the measured flowrate and pressure of steam and the product flowrate of CO_2 measured by flowmeter, assuming complete condensation of steam. Figure 4.11 shows the total heat duty per metric ton of CO_2 vs. delta loading. The data shown includes the initial test plan model results, the factorial testing, and the long-term testing at the end of the campaign lasting six weeks. The long-term data includes measurements in the morning and afternoon to determine the effect of ambient temperature on performance.

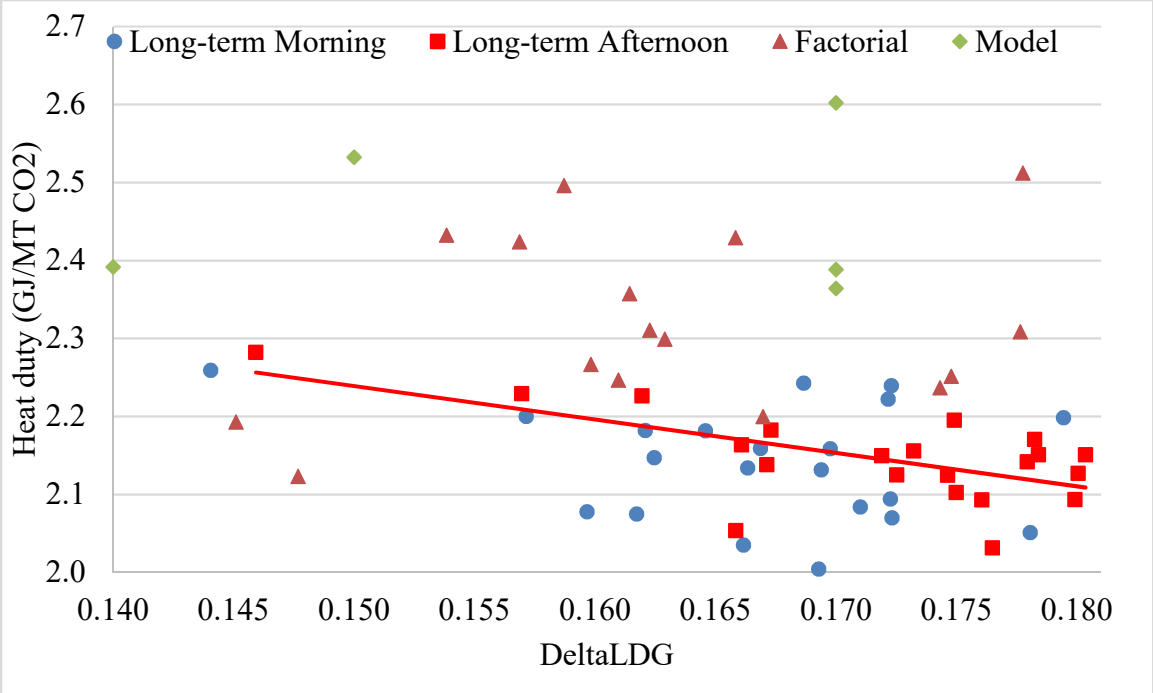

Figure 4.11: Model and experiment heat duty inversely correlated with delta loading

The heat duty was reduced with increased delta loading, due to a lower solvent rate required to strip a fixed flowrate of CO_2. Both factorial and long-term testing required lower heat rates than predicted from the modeled test cases, despite heat loss not being included in the Aspen model. Long-term morning results (07:00-08:30) showed slightly better performance than long-term afternoon results (15:00-16:30). The lower heat rates were partially caused by better heat transfer coefficients in the cross exchanger compared to predictions based on previous heat exchanger performance at SRP. The minimum heat duty required during long-term testing was 2.0 GJ/MT CO_2, with an estimated 0.2-0.3 GJ/MT CO_2 of the cost due to heat loss.

4.5.5.2 Energy balance

An energy balance was performed using the Independence model over the complete AFS to determine total heat loss. The energy balance, as previous discussed in Chapter 2, includes the rich solvent feed, lean solvent return, CO_2 product flow, condensed water, steam inlet and outlet, and cooling water inlet and outlet. The AFS is not modeled for the energy balance, only the enthalpy of the individual streams based on temperature, pressure, flowrate, and loading. The total energy input to the system is from the solvent feed, medium pressure steam, and cooling water inlet. As expected, the outlet components of the solvent have a total enthalpy greater than the inlet solvent feed, with that additional energy provided by the steam through the steam heater. While heat loss was estimated at 0.2-0.3 GJ/MT CO_2 based on previous pilot plant campaigns, the energy balance showed the majority of AFS runs to have a net heat gain. Figure 4.12 compares

the heat loss to the reboiler duty, with the lowest reboiler duty cases unsurprisingly showing the largest heat gain.

The results suggest two possible sources of the discrepancy. First, the Independence model incorrectly estimates the solvent heat capacity, heat of absorption, or both. Second, it may be possible the heat duty is underestimated due to errors in measuring the steam properties. It is possible the steam may be superheated rather than saturated vapor, thus providing additional energy beyond the heat of vaporization. While previous testing estimated the AFS reduces equivalent work by 14% compared to the simple stripper, the NCCC results suggest the AFS reduces energy requirements by nearly 30%.

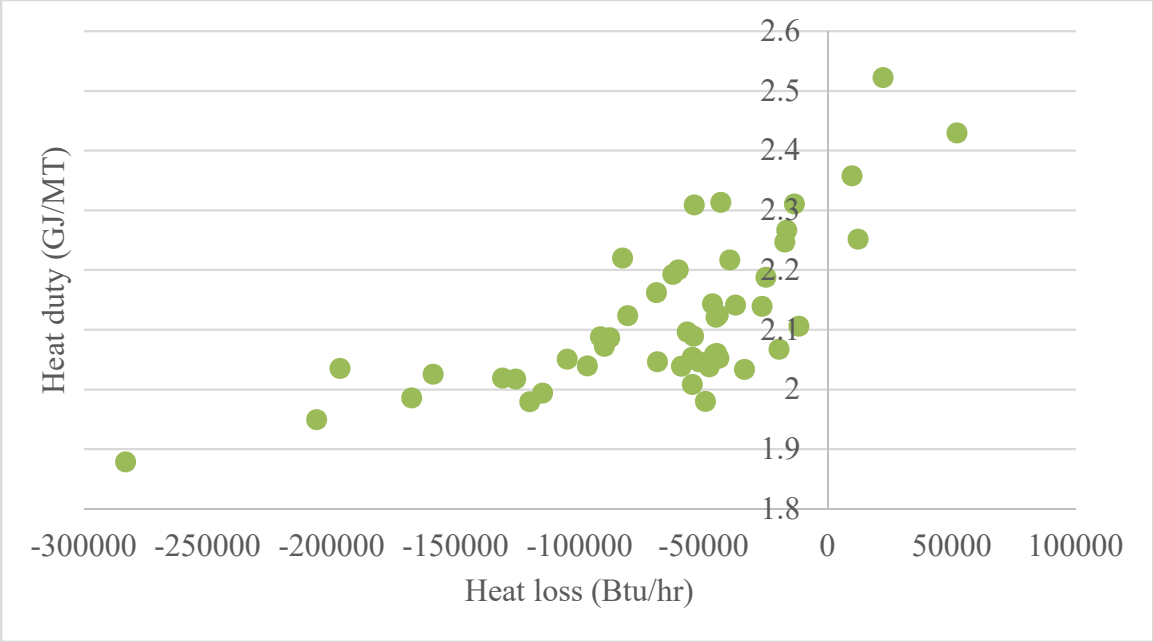

Figure 4.12: Modeled energy balance shows heat gain for 90% of AFS runs

4.5.6 Test cases

One AFS case and one simple stripper case from the NCCC campaign were fully modeled in Aspen Plus® to determine heat loss sources and estimated steam/CO_2 ratios compared to the actual measurements from the pilot plant. Both cases have similar rich and lean loadings, and Aspen Plus® models estimate similar energy requirements. The actual plant data is shown in green, and all modelled results are shown in red.

4.5.6.1 Simple Stripper

Figure 4.13 shows the simple stripper test case, with the inlet rich conditions and rich temperature measurements defined by the campaign results. The hot vapor was 6 °F colder than predicted, and the cold lean solvent was 7 °F colder; both differences were expected due to heat loss. The simple stripper model underpredicted the energy requirements by 15%.

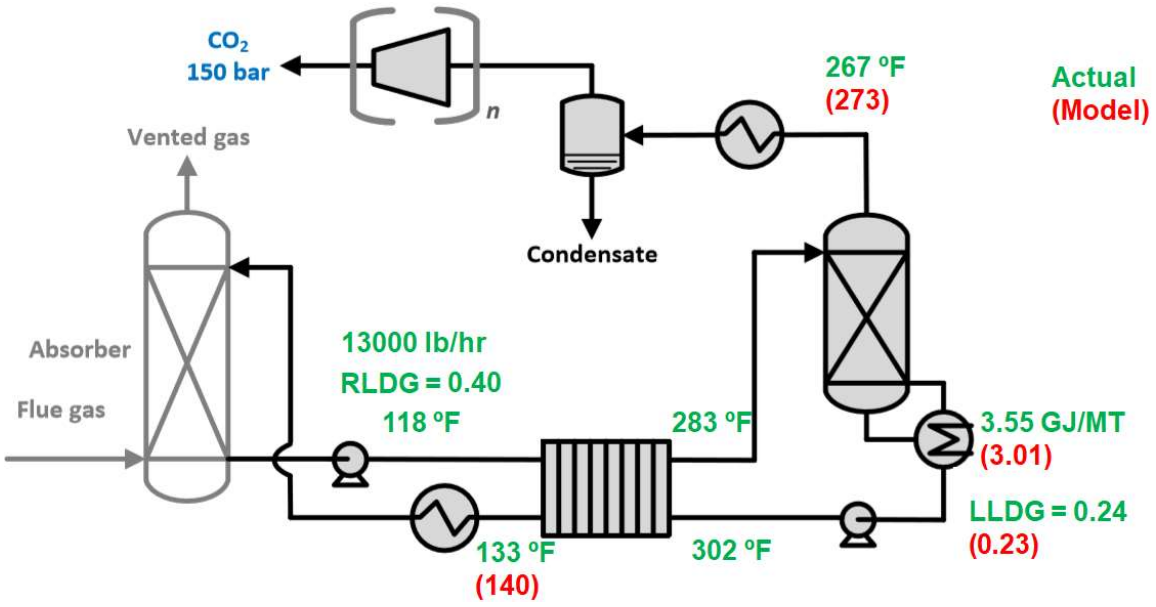

Figure 4.13: Simple stripper model underpredicts energy requirements, data from 05/29/18 07:00-08:30

4.5.6.2 Advanced Flash Stripper

The advanced flash stripper test case was modeled with three different sets of assumptions to determine the model accuracy and discrepancies for future data reconciliation. Figure 4.14 shows the AFS test case with the warm rich and hot rich temperatures assumed from the pilot results, similar to the simple stripper test case. However, the AFS model significantly underpredicts the energy requirements by over 30% compared to previous predictions by Lin (2016). The discrepancy in the hot vapor temperature is a greater factor in the AFS test case, with the temperature over 20 °F below the modeled result. The lower temperature indicates a low water mole fraction in the vapor, so there is less available latent heat for heat recovery. With reduced latent heat,

additional sensible heat is recovered in the bypass exchanger, leading to a vapor outlet temperature over 40 °F below the model predictions. This heat loss limits the benefits of the AFS configuration, which is already designed to reduce heat loss in the condenser. If heat recovery is minimal due to heat loss, capital costs could be reduced by reducing the size of the cold bypass exchanger, or even eliminating it altogether.

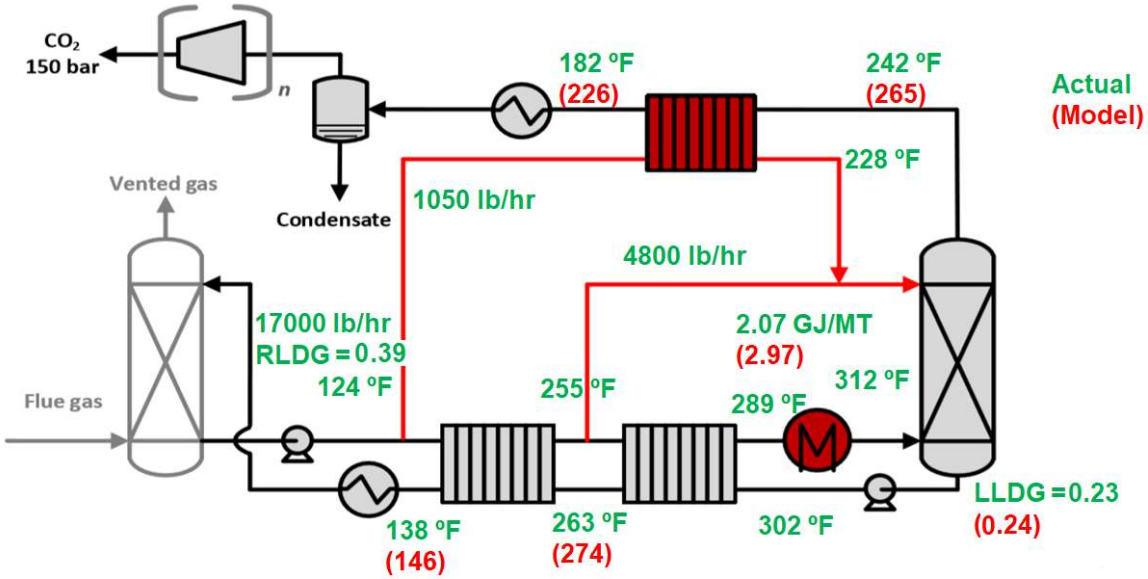

Figure 4.14: AFS model overpredicts energy requirements, data from 08/13/18 04:00-07:00

A significant cause of the energy overprediction is the temperature of the hot rich solvent entering the steam heater. Given that the vapor fraction of the rich solvent is calculated based on the solvent temperature and pressure, a slight discrepancy in the temperature reading could significantly affect the calculated heat transfer in the hot cross exchanger. The second model makes two changes from the original assumptions. First, the warm lean temperature is specified instead of the hot rich temperature. While the lean

temperature differences include some heat loss within the exchanger, there is no vaporization within the stream so the estimated heat transfer is easier to measure. Second, the temperature of the hot vapor was reduced to the measured pilot plant temperature to more accurately estimate the performance of the cold bypass exchanger.

Figure 4.15 shows the results of the second AFS model, with a reduced energy requirement of 2.45 GJ/MT CO_2. While this model still overpredicts the energy usage, the temperature of the hot rich solvent is increased by 9 °F, reducing the demand on the steam heater. The model also improves the accuracy of the cold cross exchanger and cold bypass exchanger outlet temperatures, both of which are within 3 °F of the actual results. The accuracy of the cold bypass exchange outlet is of particular interest, as it suggests the model accurately estimates the mole fraction of water in the vapor when reduced to the actual temperature.

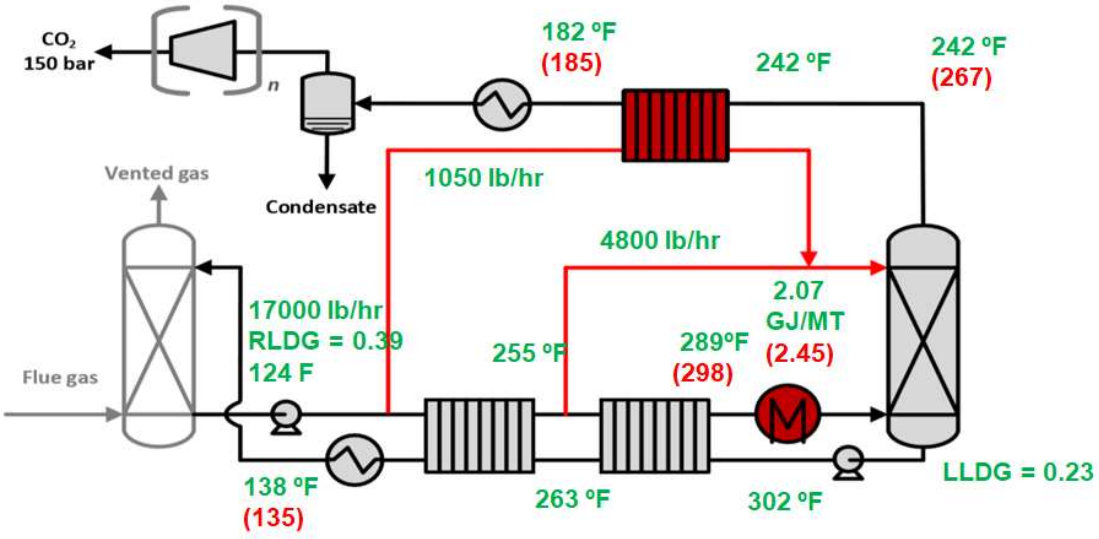

Figure 4.15: Alternate AFS model, warm temperatures specified

The third model, rather than calculating the heat duty based on the loadings, instead assumes the heat duty is correct and recalculates the loadings required to achieve it. The solvent flowrate and delta loading remain unchanged so the CO_2 product flow rate is held constant, but the rich and lean loadings are increased. Figure 4.16 shows the results of the third model, with the rich and lean loadings increased from 0.39/0.23 respectively to 0.43/0.27. To increase the lean loading, the stripper pressure was increased from 90 psia to 100 psia. Increasing the loadings by over 10% is beyond the expected error of the density-viscosity correlation and are not likely to represent the actual pilot plant results. However, the actual heat of absorption and heat capacity may be better represented by the increased loading, which can be updated through data reconciliation.

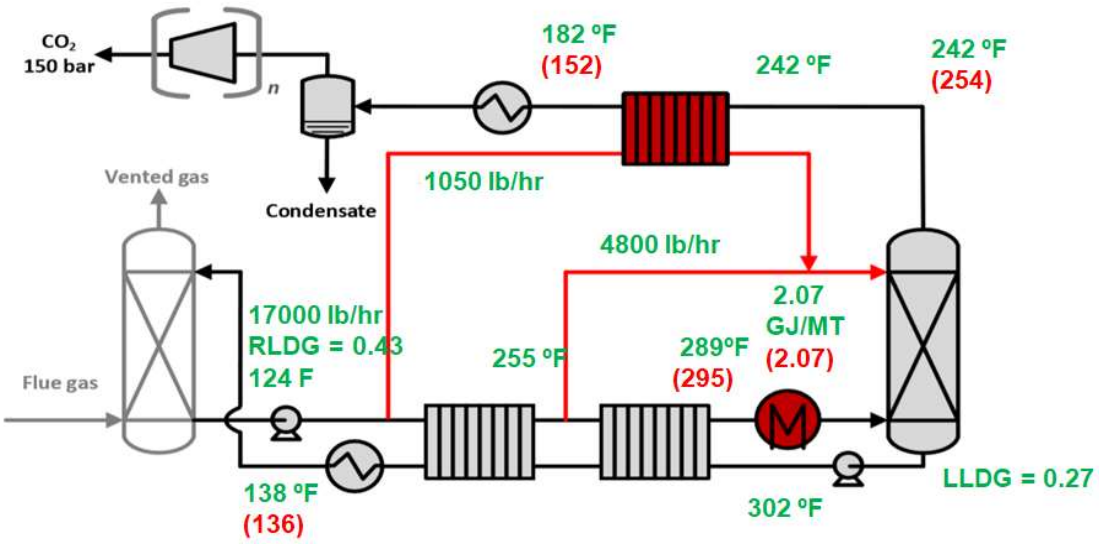

Figure 4.16: Alternate AFS model, heat duty specified

Of particular interest is the cold bypass exchanger gas outlet temperature, which the model predicts as 30 °F below the actual result. The underestimated temperature is due to very low available latent heat in the hot vapor, thus requiring additional sensible heat to provide the necessary heat transfer. This result is not representative of the actual campaign data due to the increased pressure reducing the enthalpy of the stream and limiting the benefits of heat recovery. Additional work is needed to reconcile the model with the pilot plant data to develop an improved model based on the results shown.

Chapter 5: Conclusions and Future Work

5.1 Summary of Results

5.1.1 NO_2 removal

The addition of thiosulfate and sulfite to the SO_2 prescrubber was successful in removing over 90% of the NO_2 from flue gas by inhibiting the oxidation of sulfite. The initial NO_2 removal was 98% with 60 mmol/kg sulfite, decreasing to 70% as sulfite reached 3 mmol/kg. Removal was based on both sulfite and pH, with an average pH of 8.2 maintained by intermittent addition of sodium hydroxide. Maintaining a pH at a minimum of 8.5 increased NO_2 removal by up to 8% compared to a pH of 7.5.

Given a constant feed of SO_2 in the flue gas, increasing thiosulfate reduced sulfite oxidation and increased the steady-state concentration of sulfite in the prescrubber. As thiosulfate decreased, sulfite decreased simultaneously regardless of NO_2 concentration due to oxidation from the inlet oxygen. Given 9000 lb/hr of flue gas with 5 ppm NO_2 and 40 ppm SO_2, a sulfite concentration of 25 mmol/kg is required to remove 90% of NO_2. 50 mmol/kg of thiosulfate is required to maintain steady-state sulfite at 25 mmol/kg,

Bench-scale experiments testing sulfite oxidation were combined to develop empirical correlations for NO_2 absorbed and the sulfite oxidation rate constant. Both models were updated to include additional temperature effects based on increased tests at commercial operating temperatures of 50-55 °C. Reducing the oxygen weight fraction in the flue gas was found to reduce sulfite oxidation at all concentrations of oxygen, rather than only below 5%. While adding additional thiosulfate during bench-scale experiments

showed diminishing returns in reducing sulfite oxidation, improved performance was seen at the pilot-scale due to the additional feed of SO_2 which was rapidly converted to sulfite.

5.1.2 Advanced Flash Stripper testing

The advanced flash stripper was tested using 5 m PZ at the National Carbon Capture Center, using 0.5 MW equivalent flue gas from a coal-fired power plant. Given a rich solvent feed which absorbed over 90% of CO_2 from flue gas, an average steam heater duty of 2.2 GJ/MT CO_2 was required to strip the solvent to lean conditions. Attempts to measure heat loss were unsuccessful due to an inaccurate energy balance possibly overestimating the heat of absorption of the solvent and underestimating the heat of vaporization of steam provided. The heat loss measured for the NCCC campaign ranged from 280,000 Btu/hr of heat gained to 58,000 Btu/hr of heat lost. The estimated heat loss before the campaign based on plant size and estimated solvent rate was 80,000 Btu/hr.

Attempts to develop a temperature-control heuristic for selecting bypass rates was successfully modeled using an average bypass temperature difference of 20 °F. However, attempts to apply the heuristic to the pilot plant results were unsuccessful due to heat loss at the top of the stripper, reducing the warm bypass temperature difference to -7 °F. In addition, a limited range of bypass solvent rates were tested due to the design of the control loops, which did not cover a large range of temperature differences. While the heuristic was not effective in this campaign, it may be of future value in new campaigns

if the control loops for the bypass are controlled by cascading results from temperature difference controllers.

A test case using the advanced flash stripper was analyzed using three different sets of temperature and loading assumptions, with heat duties ranging from 2.07 to 2.97 GJ/MT CO_2. Assuming the warm lean and rich solvent temperatures and calculating the hot rich solvent temperature reduced the heat duty to 2.45 GJ/MT CO_2, likely due to the model more accurately estimating the solvent vaporization percentage. Increasing both rich and lean loadings by 0.04 reduced the heat duty to match the pilot plant results, due to a combination of reduced heat of absorption and heat of vaporization of water in the stripper column.

5.2 Future Work

5.2.1 NO_2 removal

With the initial testing at NCCC complete, the next steps include the direct production of thiosulfate from colloidal sulfur and improved bench-scale sulfite oxidation analysis. The reaction of sulfur with sulfite to form thiosulfate has been studied and initial reaction rates have been calculated, but further research is needed to determine the effect of pH and agitation rate. The agitation rate is of particular interest, as colloidal sulfur particles can combine into larger solids if left unagitated. Improved testing is required to first make sure sulfur particles can be successfully dissolved into the prescrubber solution, then react to form thiosulfate while feeding a constant stream of NO_2. Initial dissolving of the sulfur in water before adding to the prescrubber may reduce

the risk of large solid formations, but the low volume may limit how much sulfur can be dissolved at one time.

To improve the bench-scale reaction rate experiments, more cases must be completed at 50-55 ℃ to measure the effects of pH and varied NO_2 flow. A significant difficulty in analyzing the flue gas with the NO_2 analyzer was the addition of water, causing the solvent to become concentrated and risk damaging the equipment. While water traps have already been added to the process, an additional drier line added to remove excess water can reduce the risk of damaging the equipment. In addition, more experiments with varied buffer concentrations and pH to measure the effects of pH on the process. Of particular interest is the change in pH over time affecting the NO_2, with varying removal rate as the pH either decreases.

5.2.2. Advanced Flash Stripper

Additional NCCC testing is planned in early 2019, which will require further analysis of the collected results. To effectively model the new runs using the Independence model, the Aspen Plus® design configuration must be updated with three additional changes. First, the heat exchanger correlations for pressure drop and the heat transfer coefficient must be updated based on the results collected in chapter 4. Second, the heat loss estimates in different components of the process must be estimated and new models developed to include them in the calculation. Third, the model must eventually be reconciled with the new NCCC results to update the heat of absorption to better match performance at higher loading.

Beyond the continued NCCC testing, further design configuration testing may be expanded to include a greater focus on capital costs. While previous designs have primarily focused on reducing equivalent work, the increase in renewable energy may reduce fossil fuel plant operation to intermittent usage based on daily energy demand. If carbon capture is only needed intermittently, alternate designs that save capital cost while slightly increasing the equivalent work may be beneficial. By the same logic, increased complexity of design such as including additional bypasses may provide a slight improvement in operating cost while requiring greater capital cost later on. Different configurations with a wide range of designs should be considered based on an annualized cost, which may result in less efficient designs still providing the best value.

Appendix A: NO_2 absorption with sulfite bench-scale analysis

A.1: BENCH-SCALE APPARATUS

A.1.1: Gas and liquid preparation

The high gas flow (HGF) apparatus previously used by Fine (2016) was adapted for continued bench-scale analysis of NO_2 absorption using sulfite and thiosulfate. The apparatus methodology is adapted from Sexton (2018).

A synthetic flue gas was created from a combination of air saturated with water, CO_2, 5000 ppm NO_2 in nitrogen, and nitrogen. Dry air was fed through a heated water saturator to maintain the water balance in the reactor. The saturated air was combined with CO_2 and NO_2 to produce a feed containing 12% CO_2 and 2-5 ppm NO_2 representing prescrubber conditions. Nitrogen was added to reduce oxygen from 21% to 3-8% in several experiments. All gas flows were controlled by mass flow controllers.

The HGF reactor was filled with 350 mL of solvent containing desired concentrations of aqueous sulfite and thiosulfate, with an additional 50 mL prepared for rinsing the reactor. Sodium carbonate and sodium bicarbonate were also added to simulate equilibrium conditions of a 10 wt % NaOH solution with 12% CO_2 flue gas, the expected operating conditions for the SO_2 prescrubber. The equilibrium conditions were estimated based on data on absorption of CO_2 into K_2CO_3 solutions from Hilliard (2008). The carbonate to bicarbonate ratio in the solution was 3:1, with an average starting pH of 9.5. For some experiments, $FeSO_4$ was added to test the effects of ferrous ions on the sulfite oxidation rate. Trace EDTA (0.02 mmol/kg) was added to most solutions to

chelate undesired metal ions, with excess EDTA added in some experiments to test the effects of EDTA on NO_2 absorption.

The solution was prepared 2-3 hours ahead of the experiment, with sulfite added shortly before starting the experiment to prevent oxidation while mixing. The reactor was rinsed with deionized water and 50 mL of solvent before adding the solvent to the reactor. When the solvent reached the operating temperature of the reactor, the experiment was started.

A.1.2: Reactor operation

The complete HGF apparatus is shown in Figure A.1. The reactor was maintained at constant temperature using a temperature-controlled circulating oil bath. The reactor operated in two configurations: "reactor" mode and "bypass" mode, controlled by 3-way valves. In both configurations, the outlet gas was diluted with excess air and fed to a Thermo Scientific model 42i trace level NO_X analyzer. The excess air was required to reduce the NO_2 concentration under the maximum allowable NO_2 concentration of 1000 ppb.

In bypass mode, the gas bypassed the reactor entirely and was fed directly to the analyzer. This setting was used at the beginning of the experiment to calibrate the analyzer and while collecting liquid samples. In reactor mode, the gas was sparged through the sulfite solution, and the outlet stream fed to the NO_2 analyzer to measure NO_2 removal. A vacuum pump was used to pull the outlet gas through the analyzer before finally venting to the fume hood. Two liquid entrainment traps were added to the HGF to

prevent water condensation within the analyzer, which could damage the reactor internals.

Each experiment lasted 1-3 hours, with seven liquid samples collected at fixed intervals. Longer experiments were required when testing highly inhibited solutions where the oxidation over a 1-hour period was not measurable. Liquid samples were collected by switching the reactor to bypass mode, then extracting a 1 mL sample of solvent from the top of the reactor. The samples were immediately mixed with 0.1 g of 35 wt% formaldehyde to form methylsulfonic acid (MSA), which does not oxidize like sulfite at room temperature. The NO_2 gas tubing was flushed with nitrogen at the end of each experiment to remove residual NO_2 from the HGF.

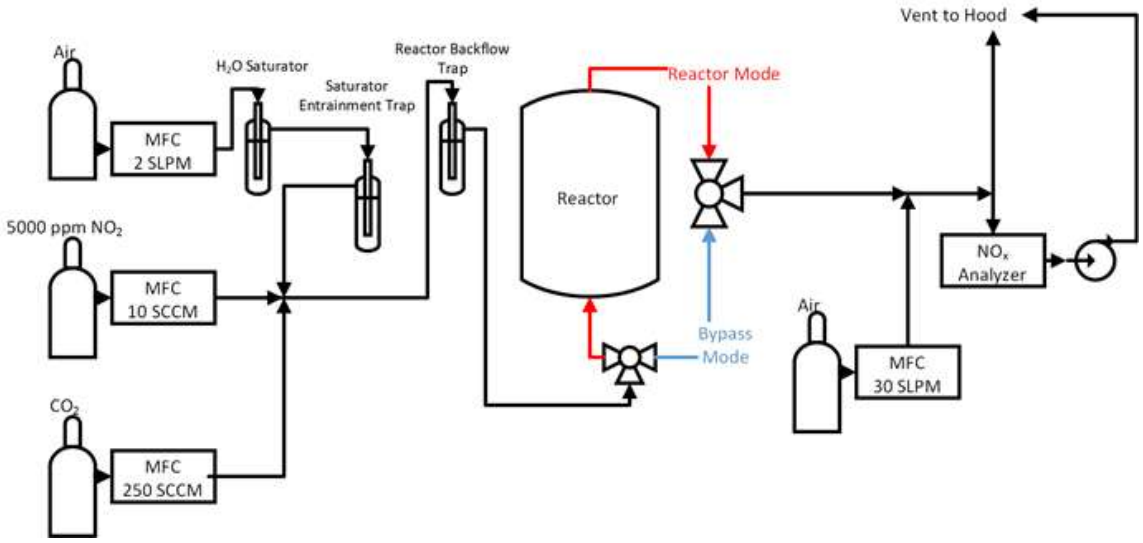

Figure A.1: High Gas Flow reactor and gas feed

A.2: LIQUID SAMPLE ANALYSIS

Liquid samples were analyzed for sulfite, sulfate, and thiosulfate concentration using anion chromatography. To prevent the oxidation of sulfite at room temperature, 0.1 g 37 wt% formaldehyde was added for every 1 g of sample. Samples were stored at room temperature for up to 3 weeks before analysis without significant sulfite oxidation. Samples were diluted by 30x with deionized water and analyzed using a Dionex ICS-3000 anion chromatography with an IonPac AS15 column.

The anion chromatograph uses a KOH eluent from 15 to 50 mM to characterize sulfite, sulfate, and thiosulfate. The concentration gradient used is shown in Figure A.2.The KOH concentration is increased from 15 to 45 mM to elute the final thiosulfate peak and improve peak separation of MSA and sulfate. The peaks were integrated and calibrated using of sulfite, sulfate, and thiosulfate standards.

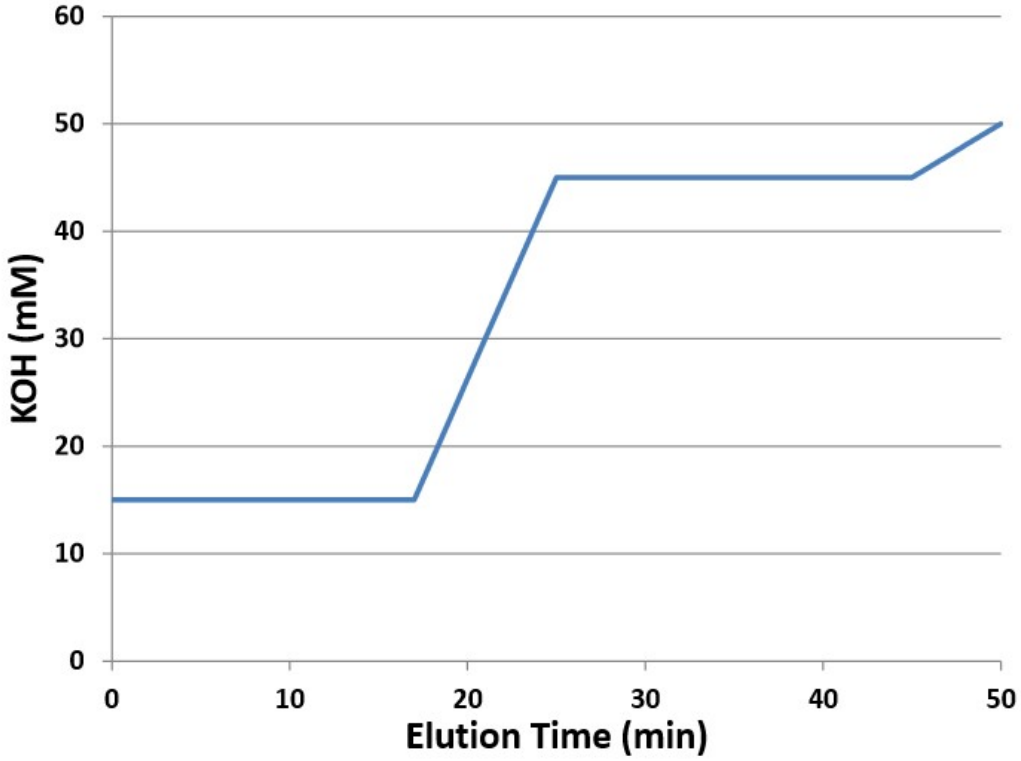

Figure A.2: KOH eluent concentration gradient for sulfite analysis

Appendix B: NCCC AFS Overview Screenshots

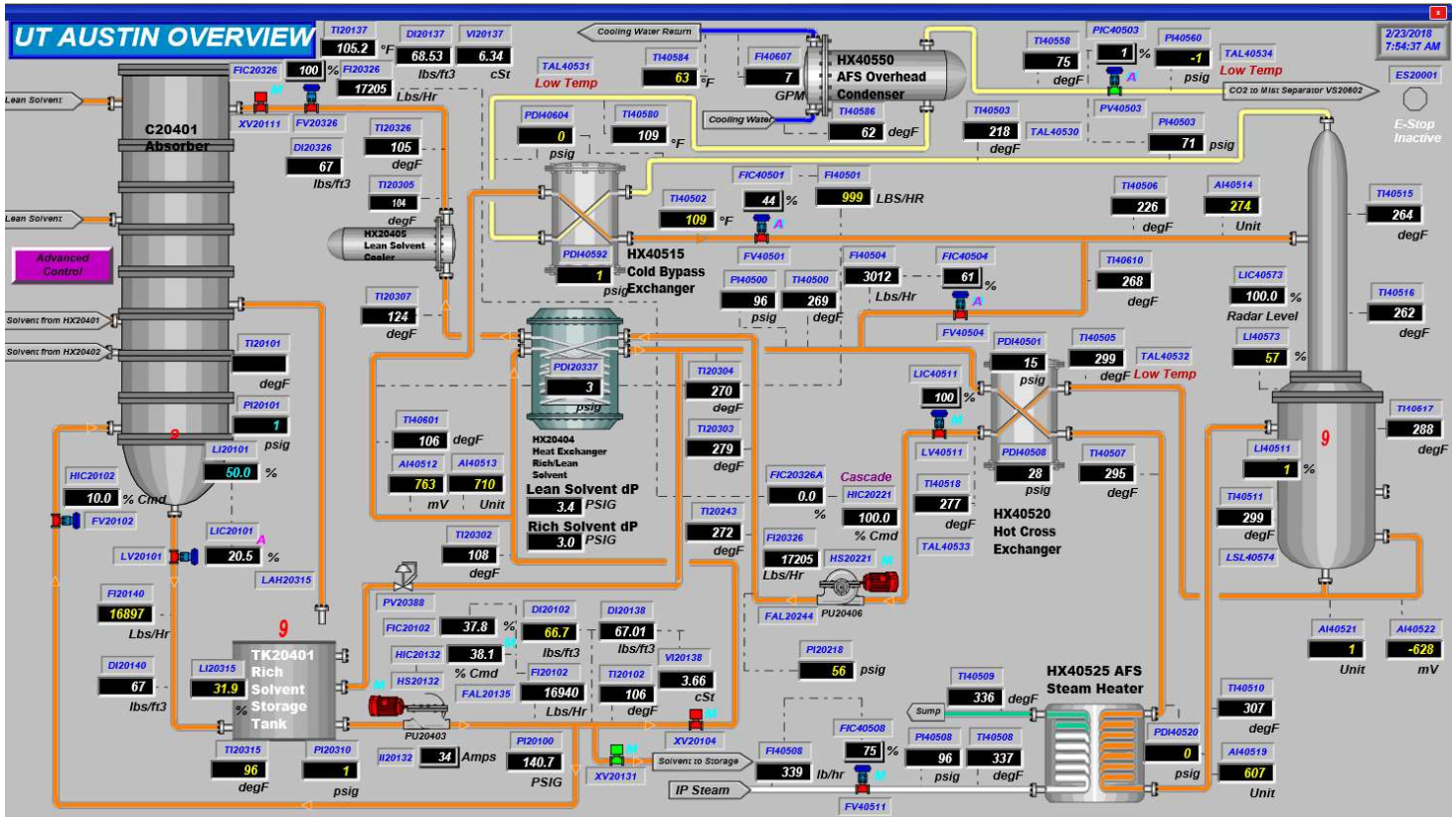

Figure B.1: Screenshot of the NCCC overview control screen for the advanced flash stripper.

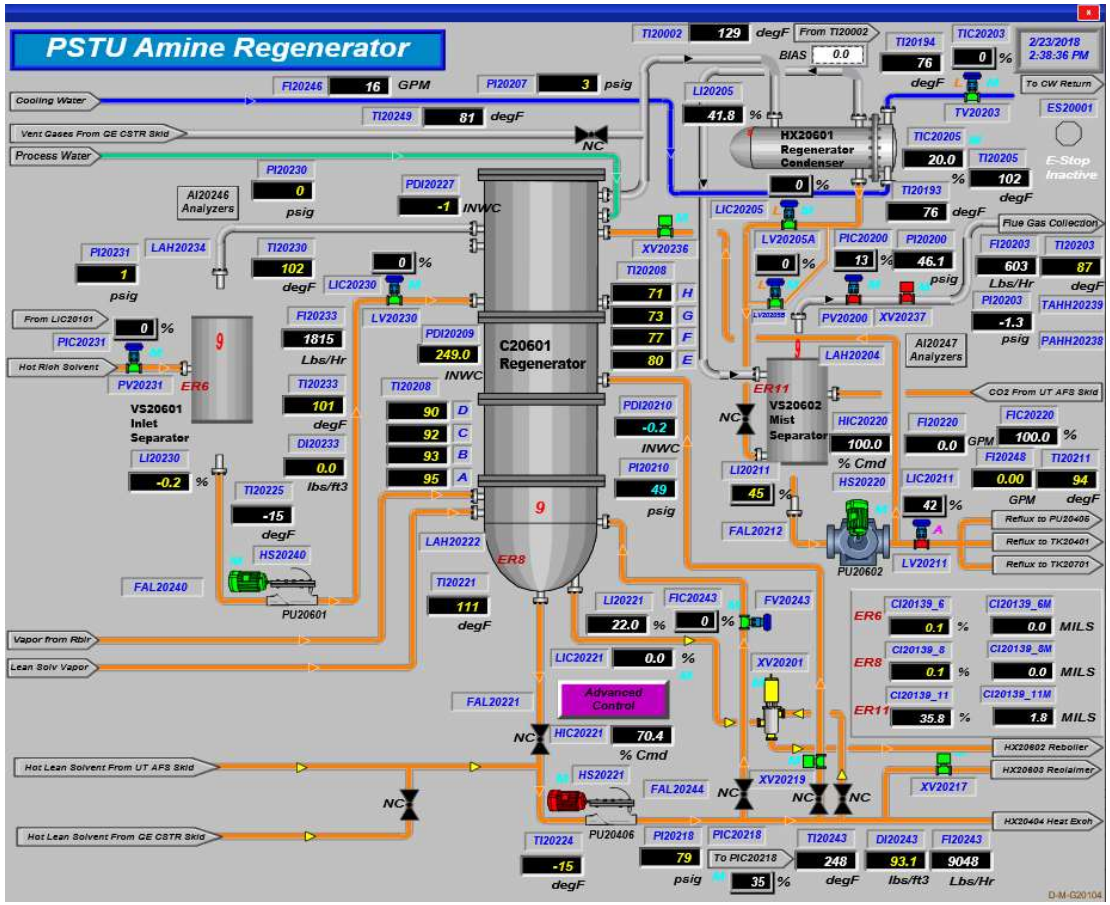

Figure B.2: Screenshot of the NCCC overview control screen for the simple stripper. The AFS cooled CO_2 product is fed to the mist separator VS20602 where the liquid condensate is removed and the purified CO_2 flowrate is measured.

References

Beaudry MR. *Aerosol Measurement and Mitigation in CO_2 Capture by Amine Scrubbing*. The University of Texas at Austin. Ph.D. Dissertation. 2018.

Bottoms. R. *Patent No. 1,783,901*. United States of America. December 2, 1930.

Chen E, Fulk SM, Sachde D, Lin YJ, Rochelle GT. "Pilot Plant Activities with Concentrated Piperazine". *Energy Procedia*, 2014;63:1376–1391.

Chen E, Zhang Y, Lin YJ, Nielsen P, Rochelle GT. "Review of Recent Pilot Plant Activities with Concentrated Piperazine". *Energy Procedia*, 2017;114:1110–1127.

Chen et al. *Advanced Flash Stripper with Concentrated Piperazine and Absorber Intercooling*. The University of Texas at Austin. Internal Report. 2017.

EIA. (2018). *Annual Energy Outlook 2018 with projections to 2050*. Annual Report. 2018.

Fine NA. *Nitrosamine Management in Aqueous Amines for Post-Combustion Carbon Capture.* The University of Texas at Austin. Ph.D. Dissertation. 2015.

Frailie PT. *Modeling of Carbone Dioxide Absorption/Stripping by Aqueous Methyldiethanolamine/Piperazine*. The University of Texas at Austin. Ph.D. Dissertation. 2014.

Freeman SA. *Thermal Degradation and Oxidation of Aqueous Piperazine for Carbon Dioxide Capture*. The University of Texas at Austin. Ph.D. Dissertation. 2011.

Garcia H, Keefer L, Lijinsky W. “Carcinogenicity of Nitrosothiomorpholine and 1-Nitrosopiperazine in Rats.” Z. Krebsforsch 1970;74: 179– 184.

Hilliard, MD. *A Predictive Thermodynamic Model for an Aqueous Blend of Potassium Carbonate, Piperazine, and Monoethanolamine for Carbon Dioxide Capture from Flue Gas.* The University of Texas at Austin. Ph.D. Dissertation. 2008

Huie RE, Neta P. “Chemical Behavior of Sulfur Trioxide SO_3^- and SO_5^- Radicals in Aqueous Solutions.” *J Phys Chem-US.* 1984;88(23):5665–5669.

Lin YJ, Chen E, Rochelle GT. “Pilot plant test of the advanced flash stripper for CO2 capture”. *Faraday Discuss*. 2016;192, 37–58.

Lin YJ, Rochelle GT. “Optimization of Advanced Flash Stripper for CO_2 Capture using Piperazine”. *Energy Procedia* 2014;63:1504–1513.

Lin YJ. *Modeling Advanced Flash Stripper for Carbon Dioxide Capture Using Aqueous Amines.* The University of Texas at Austin. Ph.D. Dissertation. 2016.

Madan T. *Modeling of Stripper Configurations for CO2 Capture using Aqueous Piperazine.* The University of Texas at Austin. M.S. Thesis. 2013.

Nash T. “The Effect of Nitrogen Dioxide and of some Transition Metals on the Oxidation of Dilute Bisulphite Solutions.” *Atmos Environ.* 1979;13(8):1149–1154.

Nielsen P. *Oxidation of Piperazine in Post-Combustion Carbon Capture*. The University of Texas at Austin. Ph.D. Dissertation. 2017.

Owens DR. *Sulfite Oxidation Inhibited by Thiosulfate.* The University of Texas at Austin. M.S. Thesis. 1984.

Plaza JM. *Modeling of Carbon Dioxide Absorption using Aqueous Monoethanolamine, Piperazine and Promoted Potassium Carbonate.* The University of Texas at Austin. Ph.D. Dissertation. 2011.

Rochelle GT. "Amine scrubbing for CO_2 capture". *Science* 2009;325:1652–1654.

Sachde D. *Absorber Performance and Configurations for CO2 Capture Using Aqueous Piperazine.* The University of Texas at Austin. Ph.D. Dissertation. 2016.

Sapkota VN, Fine NA, Rochelle GT. "NO_2-Catalyzed Sulfite Oxidation." *Ind Eng Chem Res.* 2015;54:4815–4822.

Selinger JL, Rochelle GT. "Analysis of advanced flash stripper performance using 5 m piperazine." Proceedings of GHGT-14, Melbourne, Australia. 2018

Sexton A et al. "Minimizing Solvent Oxidation with NO_2 Prescrubbing." Paper #CMTC-486336-MS. Carbon Management Technology Conference. 2017.

Shen CH. *Nitrogen Dioxide Absorption in Aqueous Sodium Sulfite*. *PhD Dissertation*. The University of Texas at Austin. 1997.

Song D. *Effect of Liquid Viscosity on Liquid Film Mass Transfer for Packings.* The University of Texas at Austin. *Ph.D. Dissertation.* 2017.

Van Wagener DH. *Stripper Modeling for CO2 Removal Using Monoethanolamine and Piperazine Solvents*. The University of Texas at Austin. Ph.D. Dissertation. 2011.

Voice, A. K. 2013. Amine Oxidation in Carbon Dioxide Capture by Aqueous Scrubbing. PhD Dissertation. The University of Texas at Austin.

Walters MS. *Dynamic Modeling of Post-Combustion Amine Scrubbing for Process Control Strategy Development*. The University of Texas at Austin. Ph.D. Dissertation. 2016.

Zhang Y, Sachde D, Chen E, Rochelle GT. "Modeling of absorber pilot plant performance for CO2 capture with aqueous piperazine." Int. J. Greenh. Gas Con. 2017. 64, 300–313.